



Early View

Original article

The mononuclear phagocyte system contributes to fibrosis in post-transplant Obliterans Bronchiolitis

Maria-Pia Di Campli, Abdulkader Azouz, Assiya Assabban, Jessika Scaillet, Marion Splittergerber, Alexandra Van Keymeulen, Frederick Libert, Myriam Remmelink, Alain Le Moine, Philippe Lemaitre, Stanislas Goriely

Please cite this article as: Di Campli M-P, Azouz A, Assabban A, *et al.* The mononuclear phagocyte system contributes to fibrosis in post-transplant Obliterans Bronchiolitis. *Eur Respir J* 2020; in press (<https://doi.org/10.1183/13993003.00344-2020>).

This manuscript has recently been accepted for publication in the *European Respiratory Journal*. It is published here in its accepted form prior to copyediting and typesetting by our production team. After these production processes are complete and the authors have approved the resulting proofs, the article will move to the latest issue of the ERJ online.

The mononuclear phagocyte system contributes to fibrosis in post-transplant Obliterans Bronchiolitis

Maria-Pia Di Campli^{1,2}, Abdulkader Azouz¹, Assiya Assabban¹, Jessika Scaillet¹, Marion Splittergerber¹, Alexandra Van Keymeulen³, Frederick Libert⁴, Myriam Remmelink⁵, Alain Le Moine¹, Philippe Lemaitre⁶ and Stanislas Goriely^{1*}

¹ Institute for Medical Immunology, Université Libre de Bruxelles, Gosselies, Belgium and ULB Center for Research in Immunology (U-CRI).

² Department of Surgery, Erasme Hospital, Université Libre de Bruxelles, Brussels, Belgium.

³ Laboratory of Stem Cells and Cancer, Université Libre de Bruxelles, Brussels, Belgium

⁴ BRIGHTcore ULB VUB and Institute of Interdisciplinary Research in Human and Molecular Biology (IRIBHM), Université Libre de Bruxelles, Brussels, Belgium

⁵ Department of Pathology, Erasme Hospital, Université Libre de Bruxelles, Brussels, Belgium.

⁶ Division of Thoracic Surgery, Lung Transplant Program, Columbia University Medical Center, New York, NY, USA.

Lead contact:

S. GORIELY, Institute for Medical Immunology, 8 rue Adrienne Bolland, B-6041 Charleroi-Gosselies, Belgium; Phone: 32-2-650-9588; Fax: 32-2-650-9563; E-mail: stgoriel@ulb.ac.be

Abstract

Bronchiolitis Obliterans Syndrome (BOS) is a fibrotic disease heavily responsible for high mortality rates after lung transplantation. Myofibroblasts are primary effectors of this fibrotic process, but their origin is still under debate. The purpose of this work was to identify the precursors of mesenchymal cells responsible for post-transplant airway fibro-obliteration.

Lineage-tracing tools were used to track or deplete potential sources of myofibroblasts in the heterotopic tracheal transplantation model. Allografts were analysed by histology, confocal microscopy, flow cytometry or single-cell transcriptomic analysis. BOS explants were evaluated by histology and confocal microscopy.

Myofibroblasts in the allografts were recipient-derived. Still, when recipient mice were treated with tacrolimus, we observed rare epithelial-to-mesenchymal transition phenomena and an overall increase in donor-derived myofibroblasts ($P=0.0467$), but the proportion of these cells remained low (7%). Hematopoietic cells, and specifically the mononuclear phagocyte system, gave rise to the majority of myofibroblasts found in occluded airways. Ablation of $Cx3cR1^+$ cells decreased fibro-obliteration ($P=0.0151$) and myofibroblasts accumulation ($P=0.0020$). Single-cell RNA-sequencing unveiled similarities between myeloid-derived cells from allografts and both murine and human samples of lung fibrosis. Finally, myofibroblasts expressing the macrophage marker CD68 were increased in BOS explants when compared to controls (14.4% vs 8.5% $P = 0.0249$).

Recipient-derived myeloid progenitors represent a clinically-relevant source of mesenchymal cells infiltrating the airways after allogeneic transplantation. Therefore, therapies targeting the mononuclear phagocyte system could improve long-term outcomes after lung transplantation.

Introduction

Lung transplantation is the only therapeutic option for selected patients with end-stage respiratory diseases. Even though an increase in terms of survival post-lung transplantation has been observed during the last decades, the proportion of patients suffering from Bronchiolitis Obliterans Syndrome (BOS), a form of chronic lung allograft dysfunction, has remained unchanged [1]. BOS, with its histologic counterpart Obliterans Bronchiolitis (OB), affects one out of two patients at 5 years post-transplant, and is heavily responsible for the limited long-term survival after lung transplantation [2]. Repetitive aggressions against the respiratory epithelium cause its progressive destruction, leading to aberrant airways fibrosis and respiratory failure [3]. A general feature of fibrotic diseases is the progressive accumulation of myofibroblasts, defined as alpha smooth muscle actin-positive (α SMA $^+$) fibroblasts that synthesize extra-cellular matrix components [4]. Their origin however remains highly controversial. They may arise from resident fibroblasts, pericytes, endothelial and epithelial cells, or circulating precursors [5–8]. The identity of these bone marrow progenitors and their connection to other myeloid cells is still elusive. Recent studies redefined the ontogeny of monocytes, macrophages and dendritic cells, which have been collectively termed as “the mononuclear phagocyte system” [9].

In the context of BOS, *ex vivo* studies concluded that myofibroblasts arise mainly from donor-derived progenitors [10, 11]. Accordingly, *in vivo* investigations, supported by *ex vivo* and *in vitro* findings [12, 13], suggested the involvement of epithelial-to-mesenchymal transition (EMT) [14]. In contrast, another study concluded that during allograft rejection, myofibroblasts were mostly recipient-derived [15].

Hence, we used genetic fate mapping strategies [4] to show that the majority of myofibroblasts in rejected grafts after heterotopic tracheal transplantation are recipient-derived, even under immunosuppression with tacrolimus. We further demonstrate that most of

these mesenchymal cells arise from myeloid precursors and that selective depletion of Cx3cR1⁺ mononuclear phagocytes decreases the accumulation of myofibroblasts and lumen fibrosis in the allografts. Finally, we identify myofibroblasts co-expressing the macrophage marker CD68 in patient samples. Collectively, these data support the involvement of myeloid-derived myofibroblasts in human BOS development after lung transplantation.

Results

Myofibroblasts in post-transplant obliterative lesions are recipient-derived.

Allogeneic heterotopic tracheal transplantation (HTT) is a widely used experimental model of BOS as it recapitulates many of its histological features and leads to a progressive intraluminal fibrotic lesion named obliterative airway disease (OAD)[16, 17]. In order to discriminate cells that are recipient- or donor-derived, we transplanted tracheas from wild-type BALB/c mice into UBI-GFP C57BL/6 mice, which express enhanced GFP under the direction of the human ubiquitin C promoter in all tissues (Figure 1a). Histological analysis of allografts at day 28 post-transplantation showed a complete loss of the epithelium which has been replaced by fibrotic tissue, whereas the syngeneic grafts from C57BL/6 wild-type donors revealed a normal pseudostratified respiratory epithelium and no fibrotic occlusion (Figure 1b). Confocal microscopy after immunofluorescent stainings showed that more than 99% of all α SMA⁺ cells in allografts lumens (defined as the area delineated by the inner edges of tracheal cartilages, which includes the submucosal space) were GFP⁺, attesting their recipient origin (Figure 1c-d). Of note, about half of these cells were stained for CD45, a hematopoietic marker.

Tacrolimus treatment reduces post-transplant obliterative lesions and allows the survival of donor-derived myofibroblasts in the allografts.

Even if these findings were in line with recent data [18], they seemed to exclude donor cells as potential sources of fibrosis, and did not fit with the conclusions of some *ex vivo* studies [10, 19]. Therefore, as a means to reduce the gap between our experimental model and the clinical settings of BOS development, we treated recipient mice with tacrolimus (FK506), an

immunosuppressant drug used in more than 80% of lung transplanted patients [2]. Previous pharmacokinetic studies in mice showed that an intraperitoneal dose of 1 mg/kg/day of tacrolimus produced blood levels in the human therapeutic range [20]. Hence, C57BL/6 Ubi-GFP recipients were treated daily with vehicle only (mock group) or 1mg/kg tacrolimus (T1 group) from day 0 to day 28 post-HTT (Figure 2a). Tacrolimus whole blood concentrations were measured using a liquid chromatography-mass spectrometry (LC-MS) assay at 3 hours post-dose (C3) (Figure 2b), and showed drug levels similar to those found in transplanted patients [21, 22]. After 28 days, histological quantification of epithelial loss and lumen occlusion revealed a significant although heterogeneous effect of tacrolimus in reducing both parameters (Figure 2c-d). Furthermore, under tacrolimus treatment, we were able to detect donor-derived GFP⁺ cells among the luminal α SMA⁺ population, even if the proportion of these cells remained generally low (7%) (Figure 2e-f). We therefore conclude that reducing the allogeneic reaction allows the survival of donor-derived mesenchymal cells that might contribute to luminal occlusion.

We next sought to test the existence of epithelial-to-mesenchymal transition phenomena under tacrolimus treatment. KRT5-Cre^{ERT2} knock-in mice on a mixed genetic background [23] were crossed with Rosa26-tdTomato reporter mice to obtain tdTomato expression in epithelial cells after tamoxifen induction (K5-TOM⁺) (Figure S1b). K5-TOM⁺ tracheas were then transplanted either into C57BL/6 wild-type (allogeneic group) or CD3ε^{-/-} recipients (considered as control non-rejected group as these mice lack T lymphocytes) and harvested 7 days after HTT, when early lesions due to alloreactivity start to appear but the epithelial layer is still preserved (Figure S1a). About 20% of tdTomato⁺ epithelial cells in the allografts expressed the mesenchymal marker α SMA⁺ (against only about 3% in the non-rejected group) (Figure S1c-d). Next, we transplanted K5-TOM⁺ tracheas into Ubi-GFP mice that were treated or not with tacrolimus (Figure S1e). At day 28 post HTT, a small fraction of epithelial-

derived (tdTomato^+) myofibroblasts (αSMA^+) (median: 1.7%; up to 14% in 2 out of 5 samples) was detected exclusively in tacrolimus-treated allografts ($P = 0.007$) (Figure S1f-g). Donor-derived (GFP^-) αSMA^+ cells with no evident epithelial origin (tdTomato^-) accounted instead for less than 10% of all myofibroblast in treated recipients. These data suggest that EMT processes might happen in allografts under circumstances of attenuated alloreactivity, but constitute only a fraction of all donor-derived mesenchymal cells.

Cells from the myeloid lineage give rise to the majority of myofibroblasts found in obliterative airways fibrosis.

Even under tacrolimus treatment, recipient cells remained the main source for intragraft myofibroblasts in our OAD model (Figure 2f), and a consistent proportion of recipient-derived αSMA^+ myofibroblasts co-expressed the hematopoietic marker CD45 (Figure 1d). Accordingly, we decided to further assess the role of recipient hematopoietic progenitors by using VAV1-CRE; Rosa26- tdTomato (VAV1-TOM) mice as recipients (Figure S2a-b) [7]. Of note, given the scarcity of recipient-derived cells infiltrating the syngeneic grafts from Ubi-GFP recipients at day 28 (Supplementary Figure S3), no further syngeneic HTT were performed in the following lineage tracing experiments. Fluorescence microscopy after nuclear (DAPI), mesenchymal (αSMA) and hematopoietic (CD45) immuno stainings indicated that more than 90% of intragraft live myofibroblasts arose indeed from tdTomato^+ hematopoietic cells (Figure S2c-d).

We next explored the hypothesis that myeloid-derived fibrocytes represent a potential source of myofibroblasts [10, 24–26]. LysMCRE;Rosa26- tdTomato recipients (LysM-TOM) were used to track myeloid cells in our HTT model (Figure 3a), and the efficiency of Cre/lox recombination was first confirmed by flow cytometry (Figure 3b) [27]. Four-color confocal

analysis showed the co-localization of α SMA, tdTomato and myeloid marker CD11b in the allografts lumen (Figure 3c). Further quantifications revealed that most of α SMA $^+$ cells in obliterative lesions derived from LysM $^+$ cells, and also indicated that almost 20% of these myeloid-derived myofibroblasts expressed the macrophage marker F4/80 (Figure 3d-e). Moreover, we noticed a positive correlation between the severity of luminal fibrosis and the proportion of myeloid-derived myofibroblasts in the allografts (Figure 3f). These results demonstrated that recipient-derived myeloid precursors were the main source of myofibroblasts in rejected airways.

The mononuclear phagocyte system represents a potential source of myofibroblasts

We therefore decided to take a closer look to LysM-lineage mesenchymal progenitors. We isolated tdTomato $^+$ cells from LysM-TOM allografts by flow cytometry and subjected these cells to single-cell RNA sequencing (scRNA-seq). TdTomato $^+$ splenocytes obtained from a LysM-TOM non-transplanted mouse were used as controls (Figure 4a).

After exclusion of contaminating lymphoid cells, we generated a two-dimensional representation of TdTomato $^+$ single cells using the Uniform Manifold Approximation and Projection (UMAP) technique [28], which revealed separation of cells into several populations (Figures 6b-c). We detected large clusters of macrophages (characterized by upregulation of *Adgre1*, *Ctsb*, *H2-Aa*, *Cd68*, *Cx3cr1*), monocytes (*Lyz2*, *Ly6c2*, *Ccr2*, *S100a4*, *Vcan*), granulocytes (*Cxcr2*, *S100a8*, *S100a9*, *Csf3r*, *MMP9*), and fibrocytes (*Lum*, *Postn*, *Colla2*, *Fn1*, *Ctgf*, *Cd34*, *Pdgfra*) (Supplementary Figure S4a). We observed clear differences between macrophages depending on their origin, such as higher expression of *Mafb*, *Mertk* and Vimentin (*Vim*) in those from the allografts (Figure 4c-d and Supplementary Figure S4b). Of note, *Mertk* and *Mafb* increased expression in macrophages has been associated with

idiopathic pulmonary fibrosis (IPF) [29, 30]. Few cells expressed *Acta2* (encoding α SMA) as samples processing and microfluidic encapsulation probably excluded fully differentiated myofibroblast (see Methods) - which in their activated form can reach up to 100 μ m of length [31, 32]. Despite this important limitation, we observed a pronounced expression of *Pdgfrb* and *Colla2* in fibrocytes and some allografts macrophages (macrophages 1) (Figure 4d and Supplementary Figure S4a). The rare population of tdTomato⁺ fibrocytes obtained from the allografts was markedly positive for a list of genes identified in human myofibroblasts from IPF patients [33] (Figure 4e). These population of myeloid-derived mesenchymal cells did not express markers of proliferation (Supplementary Figure S4d). Interestingly, the gene coding for Lumican (*Lum*) was also highly up-regulated in grafts fibrocytes (Figure 4d). Increased levels of this small proteoglycan have already been correlated with monocyte-to-fibrocyte differentiation *in vitro* and advanced disease in patients with lung fibrosis [26]. Periostin (*Postn*), a matricellular protein, was highly expressed in a group of fibrocytes (Figure 4d and Supplementary Figure S4a). In a bleomycin model, Periostin was suggested to induce myofibroblasts differentiation and lung fibrosis [34]. Moreover, the macrophages in the allografts (macrophages 1) were strongly enriched for the pro-fibrotic signature found in bleomycin-treated lungs [29] (Figure 4f).

To further investigate the link between the mononuclear phagocyte system (MPS) and airway fibrosis, we examined allografts from LysM-TOM recipients by flow cytometry and characterized myeloid-derived tdTomato⁺ α SMA⁺ cells (Figure 5a). Among these cells, the majority expressed CD11b, up to 40% co-expressed F4/80 and CD64 (two classical macrophage markers) and smaller fractions expressed Ly6C (13.8%) and Ly6G (11.1%), markers for monocytes and granulocytes, respectively (Figure 5b-c). In addition, Cx3cR1 and CD68 were highly expressed by those myeloid-derived α SMA⁺ macrophages (Figure S5b, d-e). These data, along with those obtained by confocal microscopy, support the notion that

myeloid cells, and specifically the monocyte-macrophage population, could differentiate into activated myofibroblasts in a pro-fibrogenic environment.

Cx3cR1-lineage cells express mesenchymal marker α SMA and synthetize pro-Collagen I.

Based on these results, we sought to evaluate the specific contribution of MPS by using Cx3cR1-CRE^{ERT2}; Rosa26-tdTomato (Cx3cR1^{creER}-TOM) as recipients. TdTomato expression was induced by tamoxifen-containing diet from day 0 until day 28 post-HTT, and confirmed by flow cytometric analysis on Cx3cR1^{creER}-TOM bone marrow, spleens and allografts (Figure 6a-b). Compared to the LysM-CRE system, tdTomato expression was more specific for the mononuclear phagocyte lineage, as granulocytes were not as efficiently targeted. Additionally, only a minority of T cells were tdTomato⁺. Confocal acquisition of allografts showed that 40% of α SMA⁺ cells co-localized for the fluorescent reporter tdTomato, and among these myeloid-derived myofibroblasts the majority was positive for CD45, while almost 30% expressed the macrophage marker F4/80 (Figure 6c-e). In order to assess Cx3cR1-lineage cells participation in extracellular matrix deposition, all allografts were co-labelled for pro-Collagen1A1 (proCol1A1), along with CD11b. Confocal analysis showed that most of proCol1A1⁺ cells were tdTomato⁺. This finding, combined with previous scRNAseq results, suggests that collagen production could precede cytoskeletal transformations. Moreover, approximatively 40% of all proCol1A1⁺ cells maintained the expression of CD11b, and a similar proportion was observed among the tdTomato⁺ proCol1A1⁺ population (Figure 6f-g). Overall, these data support the implication of monocyte-derived collagen-producing mesenchymal cells in luminal fibrosis post-HTT.

Ablation of Cx3cR1⁺ cells decreases fibrotic occlusion and myofibroblasts accumulation in the allografts.

To further evaluate the role of the monocyte-macrophage lineage in the fibrotic process, we induced a diphtheria toxin A (DTA)-mediated, time-controlled deletion of Cx3cR1⁺ cells in Cx3cR1-CRE^{ERT2}; Rosa26DTA (Cx3cR1-DTA) recipients. A group of Cx3cR1-DTA mice were transplanted with BALB/c tracheas and fed with tamoxifen diet (Cx3cR1-DTA^{tx}) (Figure 7a). BALB/c tracheas harvested from tamoxifen-treated C57BL/6 wild-type recipients or Cx3cR1-DTA non treated recipients were used as controls. DTA-mediated specific depletion of F4/80⁺ macrophages was verified by flow cytometric analysis (Figure 7b). Immunofluorescent stainings demonstrated a significant reduction of F4/80⁺ cells ($P = 0.007$) but also a decrease of α SMA⁺ myofibroblasts in the lumen of Cx3cR1-DTA^{tx} allografts ($P = 0.002$) (Figure 7c-d). Similarly, Masson's trichrome staining showed a reduction of lumen occlusion after Cx3cR1⁺ cells ablation ($P = 0.0151$), while there was no effect on epithelial rejection (Figure 7e). Of note, ablation of Cx3cR1⁺ cells did not affect the proportion of T cells in the spleen nor their density in the allografts (Figure 7b and f). Collectively, these data indicate that the mononuclear phagocyte system plays a central role in airway fibrosis after allogeneic transplantation.

CD68⁺ myofibroblasts are detected in fibrotic lesions from human BOS explants.

To translate our experimental findings we explored the potential role of myeloid-derived cells in human BOS fibrosis after lung transplantation. First, histological assessments confirmed the presence of typical OB lesions in the lungs from BOS patients [35], and the absence of fibrotic remodelling in control lungs (Figure 8a). Immunofluorescent staining revealed several CD45⁺ α SMA⁺ myofibroblasts in the fibro-obliterated bronchioles of rejected lungs (Figure

8b). Hence we co-stained the lungs for α SMA and CD68, a classical marker for murine (Supplementary Figure S5) and human macrophages (Figure 8c). As expected, confocal quantifications showed a general increase of α SMA⁺ cells in BOS sections (Figure 8d). Importantly, we observed a significant accumulation of CD68⁺ myofibroblasts when compared to healthy controls (14.4% vs 8.5% of all α SMA⁺ cells, $P = 0.0249$) (Figure 8e-f). Finally, the number of CD68⁺ myofibroblasts was directly related to the total number of myofibroblasts found in each lung section, suggesting that the severity of the fibrosis is correlated to the presence of myeloid-derived α SMA⁺ mesenchymal cells (Figure 8g-h). Altogether, these clinical results are consistent with our experimental findings, and imply the involvement of MPS-derived myofibroblasts in human BOS development.

Discussion

The identification of mesenchymal cells origins is a critical goal in studies on fibrotic diseases such as BOS. Here we demonstrate that the majority of myofibroblasts present in rejected allogeneic tracheas are recipient-derived. Our results are similar to those obtained in Konoeda *et al* study, where the lower contribution of recipient cells (around 75%) could be explained by several differences in experimental settings [15]. Despite limitations of the HTT model [36], these findings are in line with those obtained by Sato *et al* who used an *in vivo* model to demonstrate that almost all myofibroblasts were of extra-pulmonary origin [37]. We further show that most α SMA⁺ and collagen I-producing cells arise from myeloid precursors. Despite a large degree of heterogeneity, an important proportion of mesenchymal cells expressed typical macrophages markers.

A previous study reported that recipient-derived cells represented one third of all α SMA⁺ myofibroblasts in OB lesions [10]. However, they excluded all CD45⁺ and CD68⁺ cells during immunohistochemical assessments, therefore losing potential recipient-derived myofibroblasts of myeloid origin. Myeloid-derived mesenchymal cells found in the allografts showed very low rates of proliferation markers, confirming previous results [37]. Therefore, migration of precursors might represent the main mechanism for accumulation of myofibroblasts and extracellular matrix deposition. Once they migrate into the airways, differentiation of monocytes into macrophages can be accompanied by acquisition of mesenchymal features. In line with our hypothesis, Ishida *et al* revealed that the chemokine fractalkine promotes bleomycin-induced fibrosis by attracting Cx3cR1⁺ macrophages and fibrocytes to the lung [38]. Accordingly, an increasing number of studies suggests a major role of the mononuclear phagocyte system in chronic allograft diseases (van den Bosch et al., 2017) and pulmonary fibrosis [29, 38, 39]. Recently, a subset of pathological Cx3cR1⁺ macrophages was identified by single-cell analysis in bleomycin-induced lung fibrosis [29].

The same pro-fibrotic signature was highly activated in macrophages infiltrating the obliterated allografts in our model. Showing decreased airway luminal fibrosis upon Cx3cR1⁺-cells depletion, we confirmed the implication of the mononuclear phagocyte system in OAD. Furthermore, we demonstrate the presence of aSMA⁺ myofibroblasts co-expressing the macrophage marker CD68 in human post-transplant OB lesions, thus reinforcing the potential implication of mononuclear phagocytes in clinical OB.

Our scRNA-Seq analysis revealed the existence of a discrete population of myeloid-derived cells that express both hematopoietic and mesenchymal markers, and could represent an intermediate state between mononuclear phagocytes and α SMA^{high} myofibroblasts. Generally referred to as fibrocytes, these cells can differentiate into fibroblasts and myofibroblasts after entering the tissues [40]. This process can be associated to a loss of hematopoietic markers, such as CD45 and CD11b, making it more difficult to identify these cells with conventional techniques [7]. ScRNA-seq analysis revealed surprising similarities between mesenchymal cells from human IPF samples and fibrocytes in our BOS model [33]. High levels of Lumican and Periostin, implicated in monocyte-to-fibrocyte differentiation and myofibroblasts activation during lung fibrosis, were also detected in allograft fibrocytes [26, 34]. Furthermore, *ex vivo* studies identified a positive correlation between numbers of fibrocytes and development of BOS in lung transplanted patients, supporting the involvement of these myeloid-derived cells in OB pathogenesis [41, 42].

In a model of kidney fibrosis, LeBleu *et al* identified resident fibroblasts and non-proliferating bone-marrow progenitors as main sources of myofibroblasts, whereas epithelial cells accounted for a minor fraction (5%)[5]. Consistent with this notion, we observed an increase in donor-derived myofibroblasts and identified rare epithelial-derived aSMA⁺ cells in tacrolimus-treated allografts, a phenomenon that might be quite relevant to the clinical situation. Indeed, tacrolimus might (i) allow the survival of donor mesenchymal progenitors

such as resident fibroblasts, (ii) indirectly reduce migration of monocytes and macrophages to the graft, [43] and (iii) induce promote EMT phenomena in respiratory epithelial cells via an aberrant TGF β signalling [13, 44, 45].

In summary, our data support the involvement of cells from the mononuclear phagocyte system in human BOS development after lung transplantation. Hence, the development of specific drug delivery systems that exploit the phagocytic properties of monocytes, macrophages and myofibroblasts [31] could lead to less toxic and more efficient anti-fibrotic treatments for BOS [43].

Methods

Mice. Detailed information concerning transgenic mouse strains and reference numbers can be found in the extended Methods section of Supplementary Data. Tamoxifen citrate-containing mouse chow was used to induce Cre recombinase activity. Some of the mice received an intraperitoneal injection of 1 mg/kg/day of tacrolimus or vehicle only from transplantation until harvesting day. This study was approved by the Institutional Animal Care and Use committee of the Biopark ULB Charleroi (BUC).

Heterotopic Tracheal Transplantation model. HTT was performed by adapting the murine model developed by Hertz et al. [17] and has already been used in our laboratory as described by Lemaitre et al [16].

Human samples. All human *ex vivo* samples were obtained by Erasme Hospital biobank (BE_BERA1; Biobanque Hôpital Erasme-ULB (BERA); BE_NBWB1; Biothèque Wallonie Bruxelles (BWB); BBMRI-ERIC) with the approval of the ethics committee of Erasme Hospital, ULB, Brussels. Samples were obtained from lung explants of patients undergoing a second transplant for BOS. Specimens showing healthy peripheral tissue from patients undergoing pulmonary resection for well delimited carcinoid tumor were used as controls.

Statistical analysis. GraphPad Prism software v6.01 was used to compare two data sets (Mann-Whitney non parametric t-test) or more than two groups (Kruskal-Wallis test with Dunn's multiple comparisons test), and to establish correlations (Spearman's correlation test).

See *Supplementary Data* for detailed information on experimental procedures.

Author contributions

M-P.D.C. performed most of the experiments and analysis. J.S., A.As. and A.Az. contributed to some experiments. A.Az and M.S. performed bioinformatics analysis. M.R. and A.V.K. helped with the interpretation of data and the conception of experiments. F.L. performed NGS sample processing and preliminary analysis. M-P.D.C., P.L., A.L.M., and S.G. conceived and designed the study. S.G. supervised the whole project. M-P.D.C. and S.G. wrote the manuscript. All authors approved the final manuscript before submission.

Acknowledgments

We are grateful to Laurence Vilain, Séverine Thomas and Muriel Nguyen (Institute for Medical Immunology, ULB) and to Justine Allard and Egor Zindy (CMMI-Diapath - supported by the European Regional Development Fund and the Walloon Region) for their invaluable help. We are thankful to Benjamin Beck (IRIBHM, ULB) and Christiane Knoop (Erasme Hospital, ULB) for insightful discussions, and to Frédéric Cotton (Erasme hospital, ULB) for whole blood tacrolimus assessments.

Support statement

This study was supported by the Fonds National de la Recherche Scientifique (FRS-FNRS, Belgium), the European Regional Development Fund (ERDF) of the Walloon Region (Wallonia-Biomed portfolio, 411132-957270), the Fonds pour la Chirurgie Cardiaque and the Fonds ERASME. S.G. is a senior research associate of the FRS-FNRS. M-P.D.C. is supported by a FRIA-FNRS grant.

References

1. Chambers DC, Cherikh WS, Goldfarb SB, Hayes D, Kucheryavaya AY, Toll AE, K. Khush K, Levvey BJ, Meiser B, Rossano JW, Stehlik J. The International Thoracic Organ Transplant Registry of the International Society for Heart and Lung Transplantation: Thirty-fifth adult lung and heart-lung transplant report—2018; Focus theme: Multiorgan Transplantation. *J. Hear. Lung Transplant.* 2018; 37: 1169–1183
2. Chambers DC, Yusen RD, Cherikh WS, Goldfarb SB, Kucheryavaya AY, Khusch K, Levvey BJ, Lund LH, Meiser B, Rossano JW, Stehlik J. The Registry of the International Society for Heart and Lung Transplantation : Thirty-fourth Adult Lung And Heart-Lung Transplantation Report — 2017 ; Focus Theme : Allograft ischemic time. *J. Hear. Lung Transplant.* 2017; 36: 1047–1059.
3. Verleden SE, Sacreas A, Vos R, Vanaudenaerde BM, Verleden GM. Advances in Understanding Bronchiolitis Obliterans After Lung Transplantation. *Chest* 2016; 150: 219–225
4. El Agha E, Kramann R, Schneider RK, Li X, Seeger W, Humphreys BD, Bellusci S. Mesenchymal Stem Cells in Fibrotic Disease. *Cell Stem Cell* 2017; 21: 166–177
5. LeBleu VS, Taduri G, Teng Y, Vesselina G, Woda C, Sugimoto H, Kalluri R, Israel B, Medical D. Origin and Function of Myofibroblasts in Kidney Fibrosis. *Nat. Med.* 2013; 19: 1047–1053.
6. van Amerongen M, Bou-Gharios G, Popa E, van Ark J, Petersen A, van Dam G, van Luyn M, Harmsen M. Bone marrow-derived myofibroblasts contribute functionally to scar formation after myocardial infarction. *J. Pathol.* 2014; 214: 199–210.
7. Suga H, Rennert RC, Rodrigues M, Sorkin M, Glotzbach JP, Januszyk M, Fujiwara T,

- Longaker MT, Gurtner GC. Tracking the elusive fibrocyte: Identification and characterization of collagen producing hematopoietic lineage cells during murine wound healing. *Stem Cells* 2014; 32: 1347–1360.
8. Xie T, Liang J, Liu N, Huan C, Zhang Y, Liu W, Kumar M, Xiao R, D'Armiento J, Metzger D, Chambon P, Papaioannou VE, Stripp BR, Jiang D, Noble PW. Transcription factor TBX4 regulates myofibroblast accumulation and lung fibrosis. *J Clin Invest* 2016; 126: 3063–3079
9. Guilliams M, Ginhoux F, Jakubzick C, Naik SH, Onai N, Shraml BU, Segura E, Tussiwand R, Yona S. Dendritic cells, monocytes and macrophages: a unified nomenclature based on ontogeny. *Nat Rev Immunol* 2014; 14: 571–578.
10. Bröcker V, Länger F, Fellous TG, Mengel M, Brittan M, Bredt M, Milde S, Welte T, Eder M, Haverich A, Alison MR, Kreipe H, Lehmann U. Fibroblasts of recipient origin contribute to bronchiolitis obliterans in human lung transplants. *Am. J. Respir. Crit. Care Med.* 2006; 173: 1276–1282.
11. Yousem SA. Myofibroblasts of recipient origin are not the predominant mesenchymal cell in bronchiolitis obliterans in lung allografts. *J. Heart. Lung Transplant.* 2013; 32: 266–268.
12. Hodge S, Holmes M, Banerjee B, Musk M, Kicic A, Waterer G, Reynolds PN, Hodge G, Chambers DC. Posttransplant bronchiolitis obliterans syndrome is associated with bronchial epithelial to mesenchymal transition. *Am. J. Transplant.* 2009; 9: 727–733.
13. Borthwick LA, Parker SM, Brougham KA, Johnson GE, Gorowiec MR, Ward C, Lordan JL, Corris PA, Kirby JA, Fisher AJ. Epithelial to mesenchymal transition (EMT) and airway remodelling after human lung transplantation. *Thorax* 2009; 64: 770–777.

14. Konoeda C, Koinuma D, Morishita Y, Sano A, Nagayama K, Motomura N, Kakimi K, Miyazono J, Nakajima MR, Nicolls, Murakawa T. Epithelial to Mesenchymal Transition in Murine Tracheal Allografts: An Immunohistochemical Observation. *Transpl. Proc.* 2013; 100: 130–134.
15. Konoeda C, Nakajima J, Murakawa T. Fibroblasts of recipient origin contribute to airway fibrosis in murine tracheal transplantations. *Transpl. Int.* 2015; 28: 761–763.
16. Lemaître PH, Vokaer B, Charbonnier L, Iwakura Y, Estenne M, Goldman M, Leo O, Remmelink M, Le Moine A. Cyclosporine A Drives a Th17- and Th2-Mediated Posttransplant Obliterative Airway Disease. *Am. J. Transplant.* 2013; 1: 611–620.
17. Hertz MI, Jessurun J, King MB, Savik SK, Murray JJ. Reproduction of the obliterative bronchiolitis lesion after heterotopic transplantation of mouse airways. *Am. J. Pathol.* 1993; 142: 1945–1951
18. Watanabe S, Kasahara K, Waseda Y, Takato H, Nishikawa S, Yoneda T, Hara J, Sone T, Abo M, Kimura H, Nakao S. Imatinib ameliorates bronchiolitis obliterans via inhibition of fibrocyte migration and differentiation. *J. Heart. Lung Transplant.* 2017; 36: 138–147
19. Yousem SA, Sherer C, Fuhrer K, Cieply K. Myofibroblasts of recipient origin are not the predominant mesenchymal cell in bronchiolitis obliterans in lung allografts. *J. Heart. Lung Transplant.* 2013; 32: 266–268
20. Herbst S, Shah A, Carby M, Chusney G, Kikkeri N, Dorling A, Bignell E, Shaunak S, Armstrong-James D. A new and clinically relevant murine model of solid-organ transplant aspergillosis. *Dis. Model. Mech.* 2012; 6: 643–651
21. Kim JH, Han N, Kim MG, Kim YW, Jang H, Yun HY, Yu MY, Kim IW, Kim YS, Oh

- JM. Model based development of tacrolimus dosing algorithm considering CYP3A5 genotypes and mycophenolate mofetil drug interaction in stable kidney transplant recipients. *Sci. Rep.* 2019; 9: 1–9
22. Alloway RR, Vinks AA, Fukuda T, Mizuno T, King EC, Zou Y, Jiang W, Woodle ES, Tremblay S, Klawitter J, Klawitter J, Christians U. Bioequivalence between innovator and generic tacrolimus in liver and kidney transplant recipients: A randomized, crossover clinical trial. *PLoS Med.* 2017; 14: 1–22.
23. Van Keymeulen A, Rocha AS, Ousset M, Beck B, Bouvencourt G, Rock J, Sharma N, Dekoninck S, Blanpain C. Distinct stem cells contribute to mammary gland development and maintenance. *Nature* 2011; 479: 189–193.
24. Reilkoff RA, Bucala R, Herzog EL. Fibrocytes: emerging effector cells in chronic inflammation. *Nat Rev Immunol* 2011; 11: 427–435.
25. Andersson-Sjöland A, de Alba CG, Nihlberg K, Becerril C, Ramírez R, Pardo A, Westergren-Thorsson G, Selman M. Fibrocytes are a potential source of lung fibroblasts in idiopathic pulmonary fibrosis. *Int. J. Biochem. Cell Biol.* 2008; 40: 2129–2140.
26. Pilling D, Vakil V, Cox N, Gomer RH. TNF- α – stimulated fibroblasts secrete lumican to promote fibrocyte differentiation. *Pnas* 2015; 112: 11929–11934.
27. Meng XM, Wang S, Huang XR, Yang C, Xiao J, Zhang Y, To KF, Nikolic-Paterson DJ, Lan HY. Inflammatory macrophages can transdifferentiate into myofibroblasts during renal fibrosis. *Cell Death Dis.* 2016; 7: e2495-9
28. Becht E, McInnes L, Healy J, Dutertre CA, Kwok IWH, Ng LG, Ginhoux F, Newell EW. Dimensionality reduction for visualizing single-cell data using UMAP. *Nat.*

Biotechnol. 2019; 37: 38–47.

29. Aran D, Looney AP, Liu L, Wu E, Fong V, Hsu A, Chak S, Naikawadi RP, Wolters PJ, Abate AR, Butte AJ, Bhattacharya M. Reference-based analysis of lung single-cell sequencing reveals a transitional profibrotic macrophage. *Nat. Immunol.* 2019; 20: 163–172
30. Morse C, Tabib T, Sembrat J, Buschur KL, Bittar HT, Valenzi E, Jiang Y, Kass DJ, Gibson K, Chen W, Mora A, Benos P V., Rojas M, Lafyatis R. Proliferating SPP1/MERTK-expressing macrophages in idiopathic pulmonary fibrosis. *Eur. Respir. J.* 2019; 54: 1802441
31. Nakaya M, Watari K, Tajima M, Nakaya T, Matsuda S, Ohara H, Nishihara H, Yamaguchi H, Hashimoto A, Nishida M, Nagasaka A, Horii Y, Ono H, Iribé G, Inoue R, Tsuda M, Inoue K, Tanaka A, Kuroda M, Nagata S, Kurose H. Cardiac myofibroblast engulfment of dead cells facilitates recovery after myocardial infarction. *J. Clin. Invest.* 2017; 127: 383–401.
32. Wang S, Meng X-M, Ng Y-Y, Ma FY, Zhou S, Zhang Y, Yang C, Huang X-R, Xiao J, Wang Y-Y, Ka S-M, Tang Y-J, Chung ACK, To K-F, Nikolic-Paterson DJ, Lan H-Y. TGF- β /Smad3 signalling regulates the transition of bone marrow-derived macrophages into myofibroblasts during tissue fibrosis. *Oncotarget* 2015; 7: 8809–8822
33. Parker MW, Rossi D, Peterson M, Smith K, Sikstrom K, White ES, Connell JE, Henke CA, Larsson O, Bitterman PB. Fibrotic extracellular matrix activates a profibrotic positive feedback loop. *J. Clin. Invest.* 2014; 124: 1622–1635.
34. Ashley SL, Wilke CA, Kim KK, Moore BB. Periostin regulates fibrocyte function to promote myofibroblast differentiation and lung fibrosis. *Mucosal Immunol.* 2016; 10: 1–11

35. Stewart S, Fishbein MC, Snell GI, Berry GJ, Boehler A, Burke MM, Glanville A, Gould FK, Magro C, Marboe CC, McNeil KD, Reed EF, Reinsmoen NL, Scott JP, Studer SM, Tazelaar HD, Wallwork JL, Westall G, Zamora MR, Zeevi A, Yousem SA. Revision of the 1996 Working Formulation for the Standardization of Nomenclature in the Diagnosis of Lung Rejection. *J. Heart. Lung Transplant.* 2007; 26: 1229–1242.
36. Lama VN, Belperio JA, Christie JD, El-Chemaly S, Fishbein MC, Gelman AE, Hancock WW, Keshavjee S, Kreisel D, Laubach VE, Looney MR, McDyer JF, Mohanakumar T, Shilling RA, Panoskaltsis-Mortari A, Wilkes DS, Eu JP, Nicolls MR. Models of Lung Transplant Research: a consensus statement from the National Heart, Lung, and Blood Institute workshop. *JCI Insight* 2017; 2: 1–14.
37. Sato M, Hirayama S, Lara-Guerra H, Anraku M, Waddell TK, Liu M, Keshavjee S. MMP-dependent migration of extrapulmonary myofibroblast progenitors contributing to posttransplant airway fibrosis in the lung. *Am. J. Transplant.* 2009; 9: 1027–1036.
38. Ishida Y, Kimura A, Nosaka M, Kuninaka Y, Hemmi H, Sasaki I, Kaisho T, Mukaida N, Kondo T. Essential involvement of the CX3CL1-CX3CR1 axis in bleomycin-induced pulmonary fibrosis via regulation of fibrocyte and M2 macrophage migration. *Nat. Sci. Reports* 2017; 7: 1–12
39. Zhou X, Moore BB. Location or origin? What is critical for macrophage propagation of lung fibrosis? *Eur. Respir. J.* 2018; 51: 1800103
40. Florez-Sampedro L, Song S, Melgert BN. The diversity of myeloid immune cells shaping wound repair and fibrosis in the lung. *Regeneration* 2017; 5: 3–25
41. LaPar DJ, Burdick MD, Emaminia A, Harris DA, Strieter BA, Liu L, Robbins M, Kron IL, Strieter RM, Lau CL. Circulating Fibrocytes Correlate with Bronchiolitis Obliterans Syndrome Development Following Lung Transplantation: A Novel Clinical Biomarker.

Ann Thorac Surg 2012; 23: 1–7.

42. Andersson-Sjöland A, Erjefält JS, Bjermer L, Eriksson L, Westergren-Thorsson G. Fibrocytes are associated with vascular and parenchymal remodelling in patients with obliterative bronchiolitis. *Respir. Res.* 2009; 10: 1–11.
43. van den Bosch TPP, Kannegieter NM, Hesselink DA, Baan CC, Rowshani AT. Targeting the monocyte-macrophage lineage in solid organ transplantation. *Front. Immunol.* 2017; 8: 153.
44. McMorrow T, Gaffney MM, Slattery C, Campbell E, Ryan MP. Cyclosporine A induced epithelial-mesenchymal transition in human renal proximal tubular epithelial cells. *Nephrol. Dial. Transplant.* 2005; 20: 2215–2225.
45. Kern G, Mair SM, Noppert SJ, Jennings P, Schramek H, Rudnicki M, Mueller GA, Mayer G, Koppelstaetter C. Tacrolimus increases Nox4 expression in human renal fibroblasts and induces fibrosis-related genes by aberrant TGF-beta receptor signalling. *PLoS One* 2014; 9: 1–8.

Figures descriptions

Figure 1. Almost all intragraft myofibroblasts derive from recipient cells at day 28 post-HTT. **(a)** Experimental design: two BALB/c tracheas were subcutaneously engrafted into each UBI-GFP (C57BL/6 background) recipient to obtain a complete allogeneic mismatch (allografts). C57BL/6 donors were used to obtain syngeneic controls (syngrafts). All grafts were harvested at day 28. **(b)** Representative images of Masson's trichrome and H&E staining of tracheal syngrafts (C57BL/6 donor) and allografts (BALB/c donor) at day 28. The empty stars show mucus and cellular debris in the syngraft lumen, testifying the normal epithelial function. The black stars show complete obliteration of the allografts lumen by fibrotic tissue. The empty arrowheads show a normal pseudostratified respiratory epithelium, whereas the black arrowheads indicate the absence of epithelium on the lamina basalis. Bar scales = 200 and 40 μ m. **(c)** Representative confocal images of an allograft (BALB/c into Ubi-GFP mice) at day 28 post-HTT, showing GFP, CD45, α SMA and DAPI co-stainings. Bar scales = 200 and 20 μ m. **(d)** Quantification of recipient-derived myofibroblasts (GFP^+/α SMA $^+$) and CD45 expression among recipient-derived myofibroblasts in fibrotic airways, based on confocal pictures ($n = 6$ allografts). Data are shown as median values \pm interquartile ranges.

Figure 2. Tacrolimus inhibits OAD development and increases the proportion of donor-derived myofibroblasts at D28 post-HTT. **(a)** Experimental design: two BALB/c tracheas were implanted into an Ubi-GFP recipient. Recipients received either 1mg/kg of tacrolimus (T1) or vehicle-only (Mock) IP daily injections. All grafts were harvested at day 28 post-HTT. **(b)** Whole blood levels of tacrolimus at 3h post-dose (C3) measured by liquid-chromatography mass-spectrometry ($n = 4$ mice). **(c)** Representative histological pictures of a mock-treated allograft compared to a tacrolimus-treated allograft at day 28. Masson's trichrome and H&E stainings. The empty stars show the intraluminal fibrosis, the empty

arrowheads indicate the lamina basalis, the black stars identify the submucosal fibrosis, while the black arrowheads show the flattened respiratory epithelium. Bar scales = 50 μ m. (d) Quantification of epithelial loss and luminal occlusion in the allografts ($n = 5-7$ independent allografts). Data are shown as median values \pm interquartile ranges. (e) Representative confocal images of the allografts with or without tacrolimus treatment. The empty stars indicate the lumen. The white arrowhead points to donor-derived myoFBs, which are negative for GFP and CD45 and positive for α SMA. Nuclei are stained with DAPI. Bar scale = 30 μ m. (f) Quantification of the proportion of donor-derived myoFBs ($GFP^- \alpha$ SMA $^+$), based on confocal images. Each dot represents a BALB/c graft from an Ubi-GFP recipient at day 28 post-HTT ($n = 7 - 11$ per group). Data are shown as median values \pm interquartile ranges.

Figure 3. Recipient myeloid cells give rise to the majority of intragraft myofibroblasts.

(a) Experimental design: two BALB/c tracheas were engrafted into each LysM-Cre;Rosa26tdTomato (LysM-TOM) recipient. At day 28 post-HTT all tracheal grafts and bone marrows were harvested and analysed by confocal microscopy or flow cytometry, respectively. (b) Flow cytometry quantification of tdTomato expression in granulocytes ($CD45^+ LIN^- CD11b^+ Ly6G^+$) and monocytes ($CD45^+ LIN^- Ly6G^- CD11b^+ Ly6C^{hi}$) from LysM-TOM bone marrows ($n = 5$ mice). (c) Representative confocal pictures of a LysM-TOM allograft at day 28 post-HTT. The arrowheads in the merged lower picture show several cells colocalizing for α SMA (white), tdTomato (red) and CD11b (yellow) from a fibrotic area of the allograft lumen. Bar scales = 200 μ m and 20 μ m. (d) Detail of a fibrotic allograft where the arrowhead indicates a α SMA $^+$, tdTomato $^+$ and F4/80 $^+$ cell in the lumen. Bar scale = 10 μ m. (e) Confocal microscopy quantification of tdTomato and F4/80 expression among α SMA $^+$ myofibroblasts or myeloid-derived tdTomato $^+$ α SMA $^+$ myofibroblasts ($n = 8$ allografts). Data are expressed as median values \pm interquartile ranges. (f) Positive correlation

between the total number of α SMA⁺ cells per section and the fraction of myeloid-derived myofibroblasts ($\text{tdTomato}^+ / \alpha\text{SMA}^+$) found in allografts lumen at day 28 post-HTT. Each dot represents one allograft section analysed by confocal microscopy.

Figure 4. ScRNA-seq analysis reveals pro-fibrotic macrophages and fibrocytes populations in the allografts. (a) Experimental design: two BALB/c tracheas were transplanted into each LysM-TOM mouse and harvested after 28 days. All tdTomato^+ cells from ten allografts and one LysM-TOM spleen were FACS-sorted and analysed using 10X Genomics single-cell RNA-sequencing technique. (b) UMAP plots of spleen (green) and allografts (red) single cells, (c) segregated in eight different clusters according to their patterns of gene expression (see also Supplementary Figure S4a). (d) UMAP plots showing absolute expression (log-normalized count) of the indicated genes. (e-f) Area under the curve (AUC) distributions for specific gene-sets (gene signatures) scored on each single cell from our data set using AUCell R package [1]. The histograms represent the AUC distribution of a gene-set identified in (e) human myofibroblasts from IPF patients [2] or (f) pro-fibrotic macrophages found in bleomycin-treated lungs [3]. The UMAP plots on the left side show in blue the cells with AUC values passing the threshold, while on the right the cells are coloured in shades of red according to the AUC value for each given gene-set.

Figure 5. Phenotypic characterization of myeloid-derived α SMA⁺ cells (a) Experimental design: each LysM-TOM mouse received two BALB/c tracheas. 28 days after surgery, allografts from the same LysM-TOM recipient were pooled together and analysed by flow cytometry. (b) Gating strategy for LysM-TOM-derived allografts. (c) Relative distribution of macrophages ($\text{CD45}^+ \text{ LIN}^- \text{ EpCAM}^- \text{ CD11b}^+ \text{ Ly6G}^- \text{ Ly6C}^- \text{ F4/80}^+ \text{ CD64}^+$), monocytes

(CD45⁺ LIN⁻ EpCAM⁻ CD11b⁺ Ly6G⁻ Ly6C^{hi}), granulocytes (CD45⁺ LIN⁻ EpCAM⁻ CD11b⁺ Ly6G⁺) and other CD11b⁺ or CD11b⁻ populations among myeloid-derived (tdTomato⁺) α SMA⁺ cells from allografts at day 28 post-HTT.

Figure 6. The mononuclear phagocyte system contributes to the myofibroblast population and participates in procollagen I production. (a) Experimental design used to track the Cx3cR1⁺ lineage during allograft rejection: two BALB/c tracheas were transplanted heterotopically on each Cx3cR1-Cre^{ERT2};Rosa26tdTomato (Cx3cR1^{creER}-TOM) recipient. The expression of the fluorescent reporter tdTomato was induced by feeding the recipients with tamoxifen-containing diet from day 0 until day 28 post-HTT. At day 28, all tracheal grafts, recipients' bone marrows and spleens were harvested and analyzed by flow cytometry or confocal microscopy. (b) Flow cytometry analysis of Cx3cR1^{creER}-TOM bone marrows (n = 4), spleens (n = 4) and allografts (n = 5 samples, each dot representing two pooled allografts from the same recipient) showing tdTomato expression in granulocytes (CD45⁺ LIN⁻ CD11c⁻ CD11b⁺ Ly6G⁺), monocytes (CD45⁺ LIN⁻ CD11c⁻ Ly6G⁻ CD11b⁺ Ly6C^{hi}), macrophages (CD45⁺ LIN⁻ CD11c⁻ Ly6G⁻ CD11b⁺ Ly6C⁻ F4/80⁺), dendritic cells (CD45⁺ LIN⁻ CD11c^{hi}), natural killer cells (CD45⁺ CD3e⁻ CD19⁻ NK1.1⁺) and T cells (CD45⁺ CD3e⁺ CD19⁻ in spleens and CD45⁺ CD3e⁺ NK1.1⁻ in allografts) after 4 weeks of tamoxifen diet induction. (c) Representative confocal picture of a BALB/c allograft from a Cx3cR1^{creER}-TOM recipient at day 28 post-HTT. A detail from the graft lumen is displayed in the lower merged picture, where several cells co-localize for α SMA, tdTomato and CD45 as indicated by arrowheads. Bar scales = 200 μ m and 20 μ m. (d) Confocal microscopy quantification of tdTomato, CD45 and F4/80 expression among α SMA⁺ myofibroblasts or myeloid-derived tdTomato⁺ α SMA⁺ myofibroblasts (n = 6 allografts). (e) Representative confocal picture of the lumen of an allograft from a Cx3cR1^{creER}-TOM recipient, where the arrowheads indicates

the co-localization of α SMA, tdTomato and F4/80 in the same cell. Bar scale = 20 μ m. (f) Representative confocal picture of a Cx3cR1^{creER}-TOM-derived allograft. Several cells in the luminal fibrosis (merged figure, arrowheads) are positive for proCollagen1a1, tdTomato and CD11b. Bar scale = 20 μ m. (g) Quantification based on confocal analysis of tdTomato and CD11b expression among proCollagen1a1⁺ cells or myeloid-derived (tdTomato⁺) proCollagen1a1⁺ cells found in the lumen of allografts at day 28. Each dot represents one allograft ($n = 6$ samples). All data are expressed as median values \pm interquartile ranges.

Figure 7. Selective depletion of Cx3cR1-expressing cells is associated with reduced occlusion and decreased myofibroblasts accumulation in allografts lumen. (a) Experimental design: two BALB/c tracheas were transplanted into each Cx3cR1^{creER}-DTA recipient. The treated group (DTA Tx) was fed with tamoxifen-containing diet in order to induce diphtheria toxin A (DTA) cytosolic expression and consequent selective depletion of Cx3cR1⁺ cells. Cx3cR1^{creER}-DTA mice without tamoxifen induction and C57BL/6 wild-type mice fed with tamoxifen diet were used as recipients in the control group. At day 28, all recipients spleens and allografts were analyzed by flow cytometry, or histology and confocal microscopy, respectively. (b) Proportion of macrophages (CD3 ϵ^- CD19 $^-$ CD11c $^-$ Ly6G $^-$ CD11b $^+$ F4/80 $^+$ Ly6C $^-$), monocytes (CD3 ϵ^- CD19 $^-$ CD11c $^-$ Ly6G $^-$ CD11b $^+$ Ly6C hi) and T cells (CD3 ϵ^+ CD19 $^-$) among CD45 $^+$ splenocytes assessed by flow cytometry analysis (each point represents an individual mouse, $n = 4-7$ per group). Among the controls, black dots represent Cx3cR1^{creER}-DTA mice without tamoxifen induction, whereas blue dots correspond to C57BL/6 wild-type mice fed with tamoxifen diet. (c) Representative confocal pictures of a control allograft (Cx3cR1^{creER}-DTA recipient without tamoxifen induction) compared to an allograft from a Cx3cR1^{creER}-DTA tamoxifen-treated recipient (DTA Tx) at day 28 post-surgery. Bar scale = 200 μ m. (d) Confocal quantification of F4/80 $^+$ and α SMA $^+$ cells found in the allografts lumen as shown in picture (C). The black dots represent the allografts from

$\text{Cx}3\text{cR}1^{\text{creER}}$ -DTA recipients without tamoxifen induction, whereas the blue dots correspond to allografts from C57BL/6 wild-type recipients treated with tamoxifen. **(e)** (*Left side*) Representative pictures of Masson's trichrome stained allografts at day 28 post-transplant. A detail of the lumen at higher magnification is shown in the left corners; bar scale = 200 μm ; (*right side*) histological quantification of lumen occlusion and epithelial loss for each group of allografts ($n = 6 - 10$ allografts). **(f)** (*Left side*) Immunohistochemical staining of $\text{CD}3\epsilon^+$ T cells in allografts at day 28 post-HTT; bar scale = 250 μm ; (*right side*) histological quantification of $\text{CD}3\epsilon^+$ T cells in the lumen of allografts with DTA-mediated $\text{Cx}3\text{cR}1^+$ cells depletion *versus* controls. (e – f) The empty dots correspond to the allografts from $\text{Cx}3\text{cR}1^{\text{creER}}$ -DTA recipients without tamoxifen treatment, whereas the allografts from C57BL/6 tamoxifen-treated recipients are shown as blue dots in the control group. All data are expressed as median values \pm interquartile ranges.

Figure 8. $\text{CD}68^+$ myofibroblasts are found in human BOS explants. **(a)** Representative scans of lung sections from control patients or patients with bronchiolitis obliterans syndrome (BOS). The higher magnification picture shows a bronchiole (Br) with typical OB lesions, next to a small pulmonary artery (A). The black arrowhead in the bronchiole lumen indicates a polypoid plaque of dense scar tissue and the absence of epithelial layer. H&E staining. Bar scales = 5 mm and 250 μm . **(b)** Representative confocal pictures showing OB lesions in the explanted lung from a BOS patient. In the merged picture on the right side, the white arrows indicate cells co-staining for αSMA and $\text{CD}45$ in the fibrotic lesion. Bar scale = 200 μm . **(c)** Representative confocal pictures of healthy human lung tissue and a BOS explant co-stained for αSMA and $\text{CD}68$. Br: bronchiole; white arrowhead: αSMA^+ smooth muscle cells; empty arrowhead: $\text{CD}68^+$ cell; white arrows: $\alpha\text{SMA}^+ \text{CD}68^+$ myofibroblasts in the BOS explant. Bar scale = 200 μm . **(d - f)** Confocal analysis quantification for: **(d)** the total number of αSMA^+

myofibroblasts, (e) α SMA⁺ CD68⁺ myofibroblasts, and (f) the fraction of α SMA⁺ cells that colocalize for CD68, in healthy lungs versus BOS explant. All α SMA⁺ smooth muscle cells were excluded from the count. Each dot represents the mean value of four random fields (200x) quantified for each sample ($n = 7 - 10$ patients per group). The central bar represents the median value. (g) Confocal quantification of the fraction of α SMA⁺ cells colocalizing for CD68 (red part of column) in each explant (BOS) or control sample. Four random fields (200x) were analysed for each sample (mean value shown). (h) Positive correlation between the total number of α SMA⁺ myofibroblasts and the fraction of CD68⁺ myofibroblasts found in human lungs (BOS and controls). Each dot represents the mean value of four random fields from the same sample ($n = 17$ patients).

Supplementary Figure S1. EMT phenomena are found in the allografts at early stages of OAD and at later stages under tacrolimus treatment. (a) Experimental design: two tracheas from K5-Cre^{ERT2};Rosa26tdTomato (K5-TOM) mice were transplanted into each C57BL/6 wild-type mouse in the allografts group, or into each CD3 $\varepsilon^{-/-}$ mouse (CD3 ε KO) in the "non-rejected grafts" group. All K5-TOM donors were fed with tamoxifen-containing diet to induce tdTomato expression in K5⁺ epithelial lineage. All grafts were harvested at day 7 post-HTT. (b) Cre/Lox efficiency tested on K5-TOM native tracheas by confocal microscopy after 3 weeks of tamoxifen-containing diet. Each data point represent one complete section of trachea. Four different sections were examined for each trachea ($n = 2$ mice). (c) Representative confocal images of a non-rejected graft compared to an allograft at day 7. The white arrowheads show several tdTomato⁺ cells in the epithelial layer of the allograft that co-stain for α SMA. Bar scale = 200 μ m. (d) Confocal analysis quantification showing the fraction of tdTomato⁺ cells that colocalize for α SMA in grafts lumen at day 7 ($n = 5-7$ grafts). (e) Experimental design: two K5-TOM tracheas were engrafted into each Ubi-GFP mouse.

TdTomato expression was induced by tamoxifen-containing diet for 3 weeks. All recipients received either 1mg/kg tacrolimus (T1) or mock IP injections every day until grafts harvesting at day 28 post-HTT. **(f)** Representative confocal pictures of a tacrolimus-treated allograft at day 28. The white arrowheads indicate some tdTomato⁺ αSMA⁺ cells found in the lumen. Bar scale = 200 μm. **(g)** Confocal analysis quantification of tdTomato expression among luminal αSMA⁺ cells in mock and T1-treated allografts. Each dot represents one graft (n = 5-8). All data are shown as median values ± interquartile ranges.

Supplementary Figure S2. Most myofibroblasts arise from recipient-derived hematopoietic cells. **(a)** Experimental design: two BALB/c tracheas were implanted subcutaneously into each VAV1-Cre;Rosa26tdTomato (VAV1-TOM) recipient in order to specifically track the recipient-derived hematopoietic lineage (tdTomato⁺ cells). All allografts and recipients bone marrows were harvested at day 28 post-HTT and analysed respectively by confocal microscopy or flow cytometry. **(b)** Flow cytometry analysis of VAV1-TOM bone marrows (n = 3 mice): quantification of tdTomato expression among CD45⁺ hematopoietic cells (left) and CD45 expression among all tdTomato⁺ cells (right). **(c)** Representative confocal images of allografts (BALB/c to VAV1-TOM) at day 28, showing αSMA, tdTomato, CD45 and DAPI co-staining. Bar scale = 200 μm. **(d)** Proportion of αSMA⁺ myofibroblasts expressing the hematopoietic reporter tdTomato in the lumen fibrosis at day 28, based on confocal analysis (n = 6 allografts).

Supplementary Figure S3. Confocal analysis of syngeneic grafts from UbiGFP recipients at day 28 post-HTT. **(a)** Experimental design. **(b)** Confocal images of a syngeneic graft (C57BL/6 trachea into Ubi-GFP recipient) at day 28 after transplantation (representative of 3

independent experiments). The arrows show some GFP⁺ recipient-derived cells in the submucosa. Bar scale = 200 μ m.

Supplementary Figure S4. ScRNA-seq analysis of tdTomato⁺ cells from LysM-TOM spleen and allografts. (a) Dot plots showing average expression of selected lineage-defining genes across identified clusters [4–6]. (b) Heatmap of genes differentially expressed between the “Macrophages 1” (mainly allograft cells) and “Macrophages 2” (mainly splenocytes) clusters. (c) UMAPs showing the expression of several genes of interest across different clusters. (d) Dot plots representing the expression of specific markers of cell proliferation [7] among each cluster.

Supplementary Figure S5. Phenotypic characterization of myeloid-derived α SMA⁺ cells by flow cytometry. (a) Experimental design. The two allografts harvested from the same recipient at day 28 were pooled together before performing flow cytometric analysis. (b) Gating strategy for LysM-TOM-derived allografts. (c) Proportion of α SMA⁺ cells expressing or not the myeloid reporter tdTomato among either CD45⁺ Lin⁻ or CD45⁻ Lin⁻ cells. (d) Proportion of Cx3cR1-expressing macrophages (CD45⁺ LIN⁻ CD11b⁺ Ly6G⁻ Ly6C⁻ F4.80⁺), monocytes (CD45⁺ LIN⁻ CD11b⁺ Ly6G⁻ Ly6C^{hi}) and granulocytes (CD45⁺ LIN⁻ CD11b⁺ Ly6G⁺) among myeloid-derived (tdTomato⁺) α SMA⁺ cells. All data are shown as median values \pm interquartile ranges. (e) Relative distribution of CD68⁺ Cx3cR1⁺ or Cx3cR1⁻ macrophages (CD45⁺ LIN⁻ CD11b⁺ Ly6G⁻ Ly6C⁻), monocytes (CD45⁺ LIN⁻ CD11b⁺ Ly6G⁻ Ly6C^{hi}), granulocytes (CD45⁺ LIN⁻ CD11b⁺ Ly6G⁺) and other CD11b⁺ or CD11b⁻ populations among myeloid-derived (tdTomato⁺) α SMA⁺ cells from allografts at day 28 post-HTT. (c – e) Each dot or bar represents two pooled allografts from the same LysM-TOM recipient (n = 5).

References

1. Aibar S, González-Blas CB, Moerman T, Huynh-Thu VA, Imrichova H, Hulselmans G, Rambow F, Marine JC, Geurts P, Aerts J, Van Den Oord J, Atak ZK, Wouters J, Aerts S. SCENIC: Single-cell regulatory network inference and clustering. *Nat. Methods* 2017; 14: 1083–1086.
2. Parker MW, Rossi D, Peterson M, Smith K, Sikstrom K, White ES, Connell JE, Henke CA, Larsson O, Bitterman PB. Fibrotic extracellular matrix activates a profibrotic positive feedback loop. *J. Clin. Invest.* 2014; 124: 1622–1635.
3. Aran D, Looney AP, Liu L, Wu E, Fong V, Hsu A, Chak S, Naikawadi RP, Wolters PJ, Abate AR, Butte AJ, Bhattacharya M. Reference-based analysis of lung single-cell sequencing reveals a transitional profibrotic macrophage. *Nat. Immunol.* 2019; 20: 163–172
4. Cohen M, Giladi A, Gorki AD, Solodkin DG, Zada M, Hladik A, Miklosi A, Salame TM, Halpern KB, David E, Itzkovitz S, Harkany T, Knapp S, Amit I. Lung Single-Cell Signaling Interaction Map Reveals Basophil Role in Macrophage Imprinting. *Cell* 2018; 175: 1031–1044
5. Scott CL, T'Jonck W, Martens L, Todorov H, Sichien D, Soen B, Bonnardel J, De Prijck S, Vandamme N, Cannoodt R, Saelens W, Vanneste B, Toussaint W, De Bleser P, Takahashi N, Vandenabeele P, Henri S, Pridans C, Hume DA, Lambrecht BN, De Baetselier P, Milling SWF, Van Ginderachter JA, Malissen B, Berx G, Beschin A, Saeys Y, Guiliams M. The Transcription Factor ZEB2 Is Required to Maintain the Tissue-Specific Identities of Macrophages. *Immunity* 2018; 49: 312–325.
6. Schyns J, Bai Q, Ruscitti C, Radermecker C, Schepper S De, Chakarov S, Farnir F, Pirottin D, Ginhoux F, Boeckxstaens G, Bureau F, Marichal T. Non-classical tissue

monocytes and two functionally distinct populations of interstitial macrophages

populate the mouse lung. *Nat. Commun.* 2019; 10: 3964

7. Morse C, Tabib T, Sembrat J, Buschur KL, Bittar HT, Valenzi E, Jiang Y, Kass DJ, Gibson K, Chen W, Mora A, Benos P V., Rojas M, Lafyatis R. Proliferating SPP1/MERTK-expressing macrophages in idiopathic pulmonary fibrosis. *Eur. Respir. J.* 2019; 54: 1802441

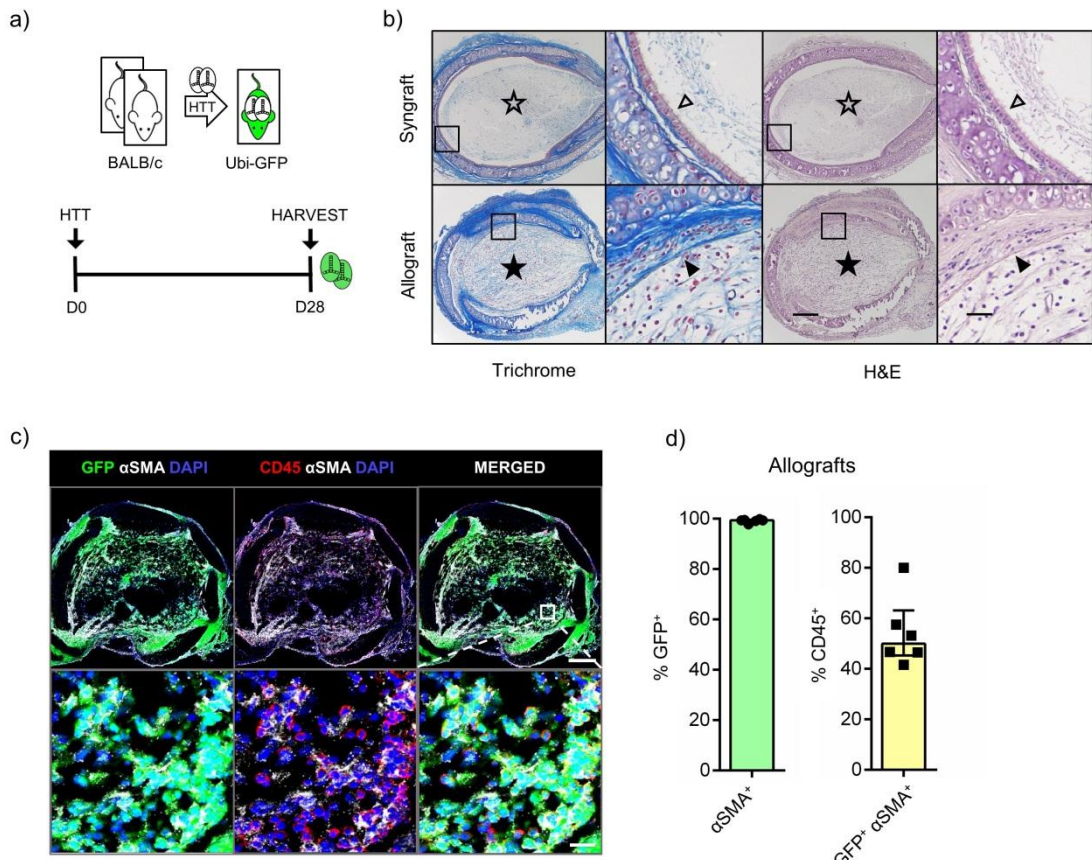


Figure 1. Almost all intragraft myofibroblasts derive from recipient cells at day 28 post-HTT.

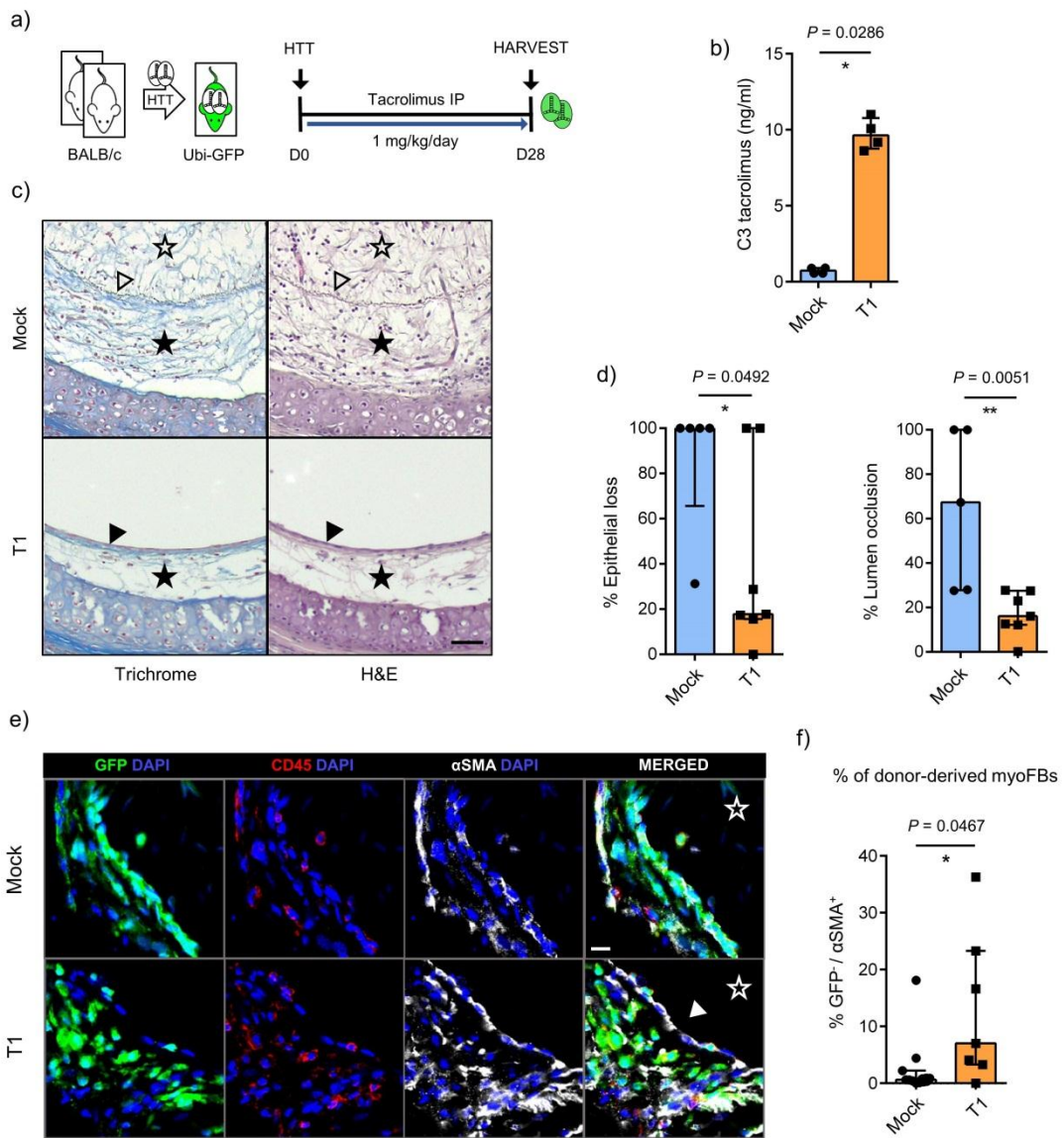


Figure 2. Tacrolimus inhibits OAD development and increases the proportion of donor-derived myofibroblasts at D28 post-HTT.

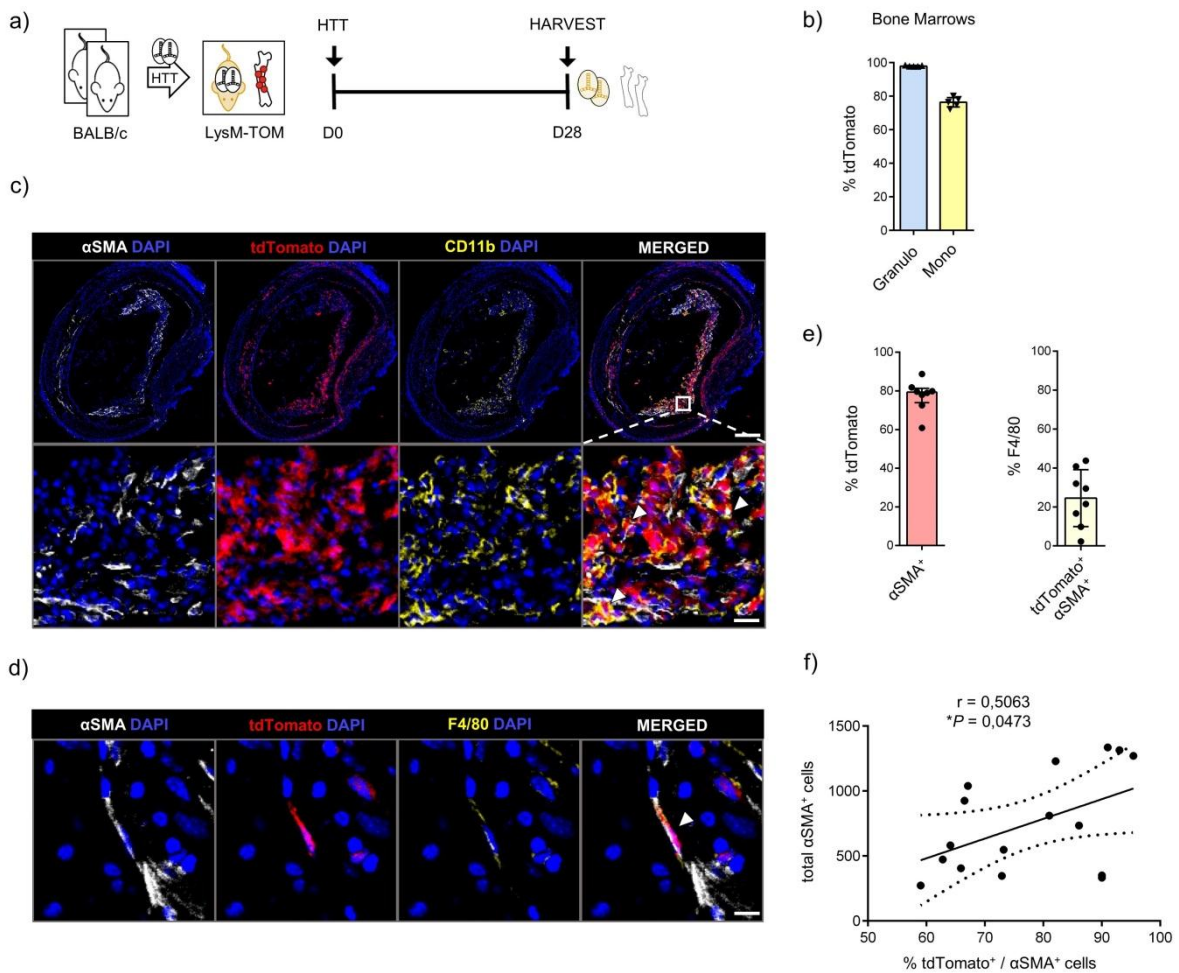


Figure 3. Recipient myeloid cells give rise to the majority of intragraft myofibroblasts.

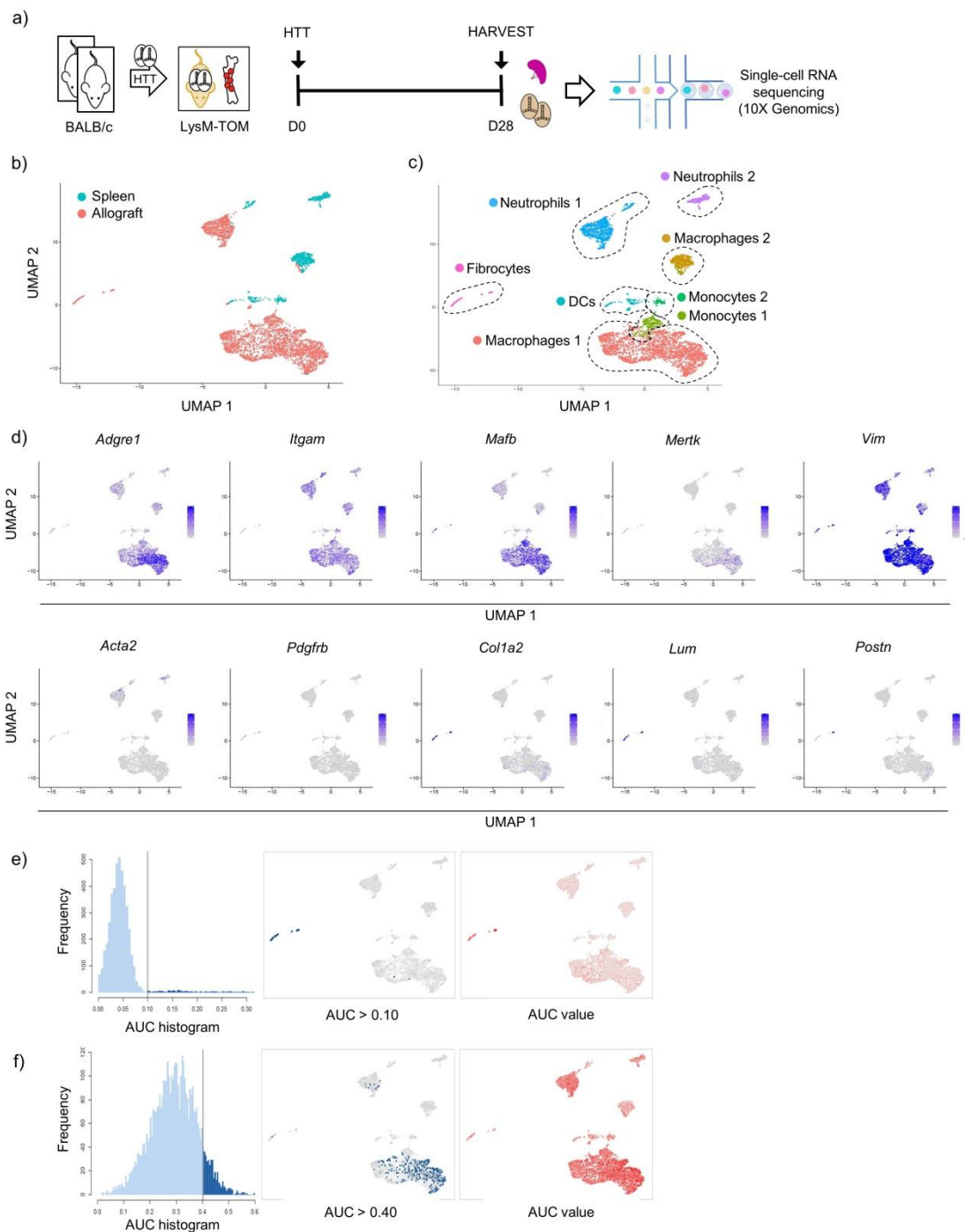


Figure 4. ScRNA-seq analysis reveals pro-fibrotic macrophages and fibrocytes populations in the allografts.

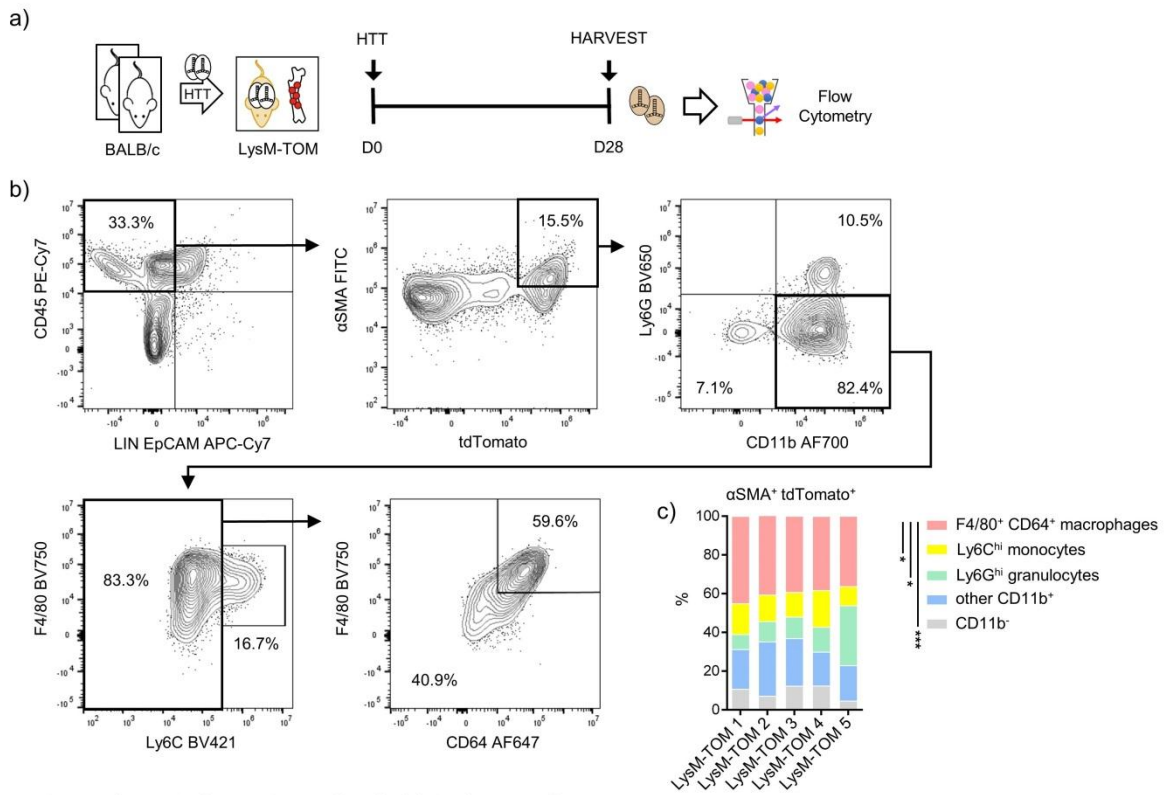


Figure 5. Phenotypic characterization of myeloid-derived α SMA⁺ cells

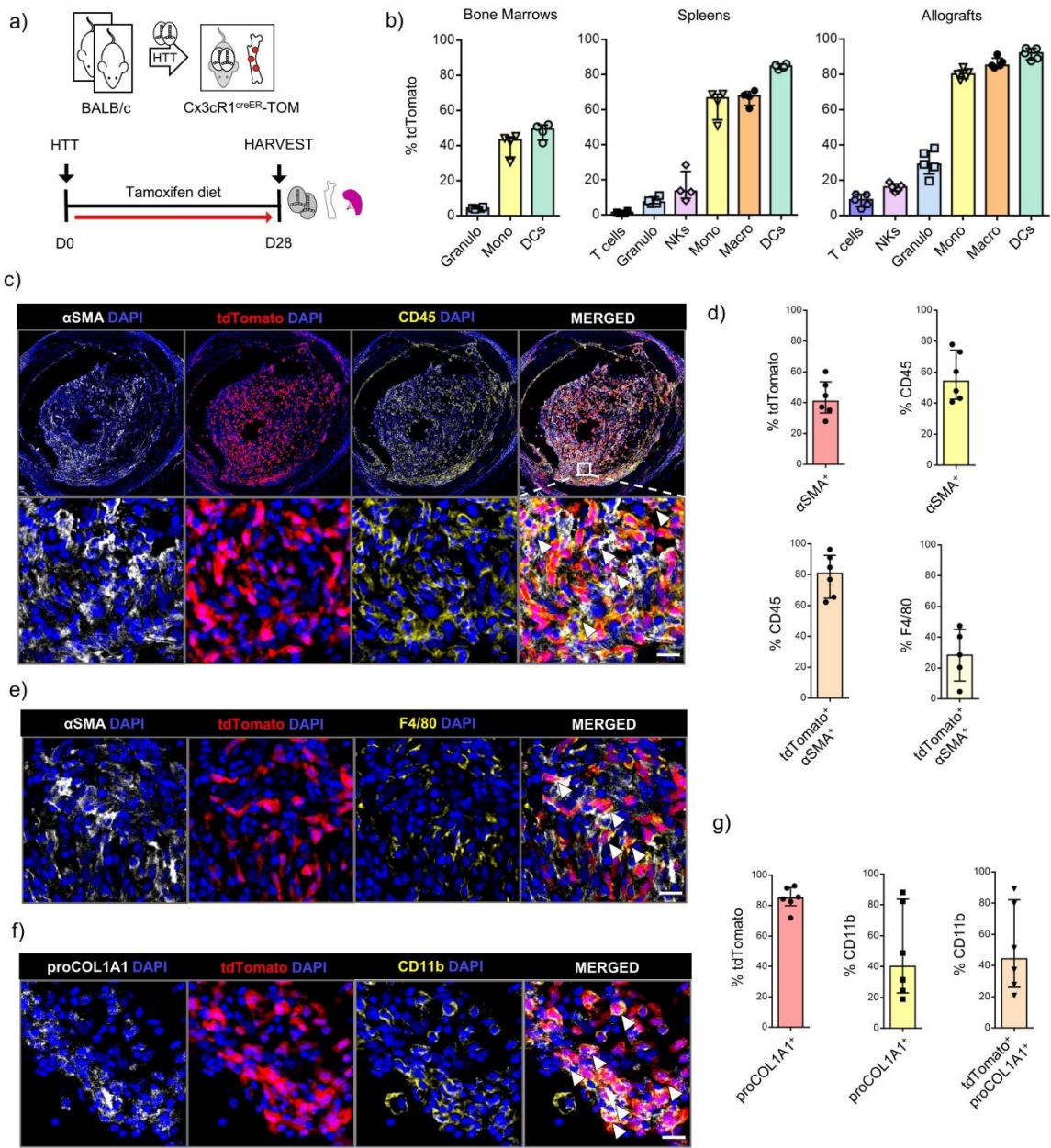


Figure 6. The mononuclear phagocyte system contributes to the myofibroblast population and participates in procollagen I production.

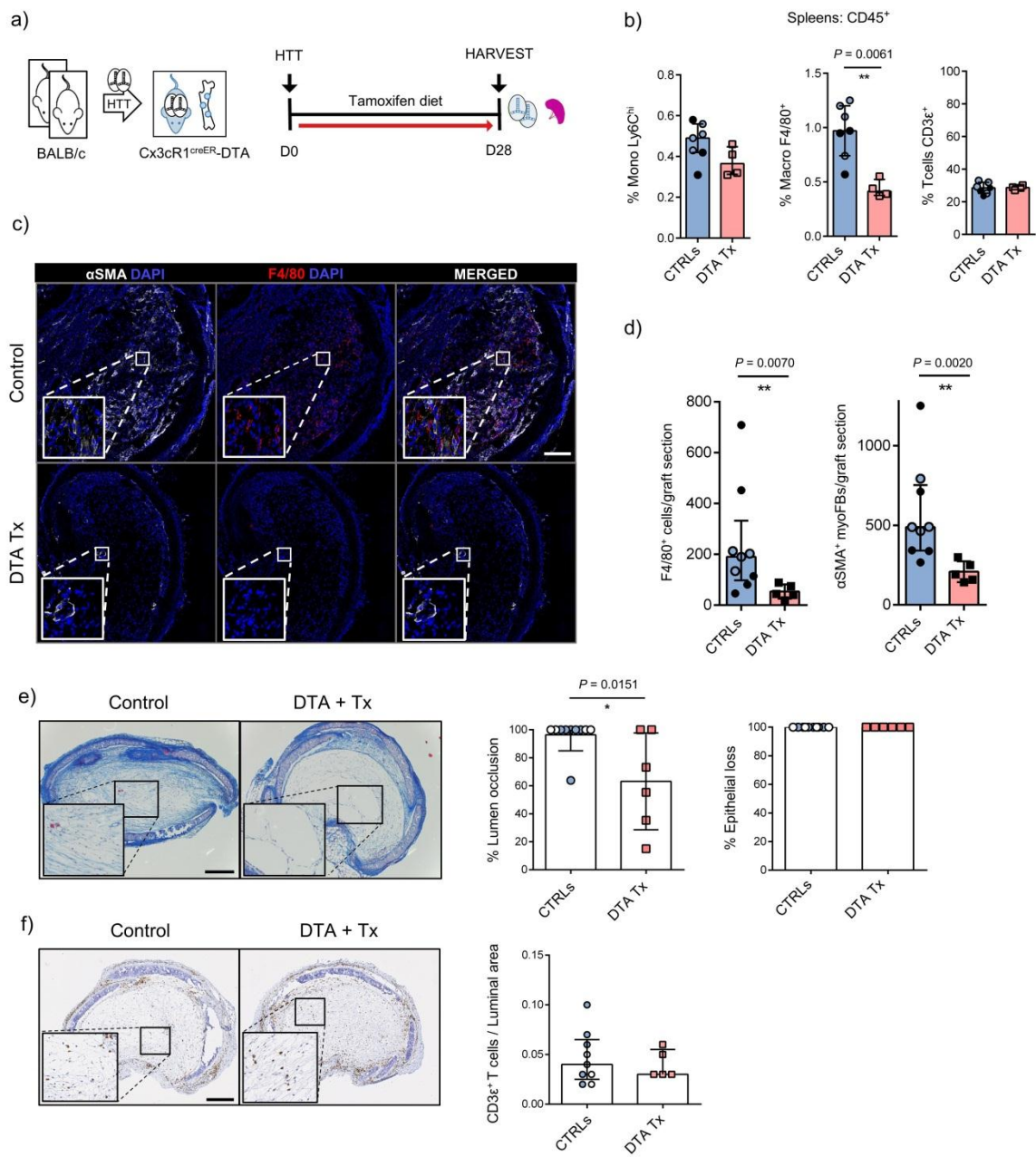


Figure 7. Selective depletion of Cx3cR1-expressing cells is associated with reduced occlusion and decreased myofibroblasts accumulation in allografts lumen.

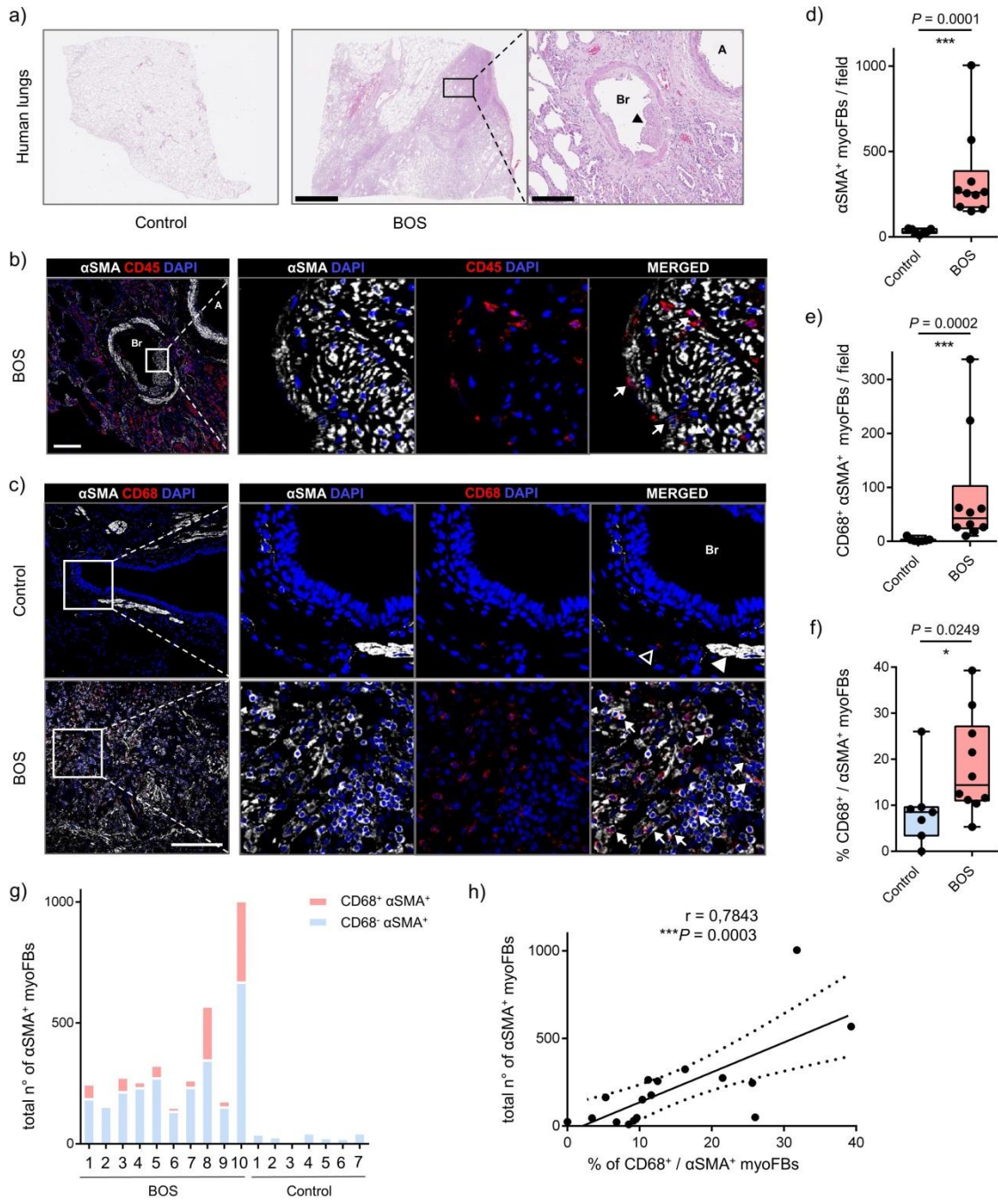


Figure 8: CD68⁺ myofibroblasts are found in human BOS explants.

Supplementary data

Methods: extended version

Mice. Wild-type Balb/c (BALB/cOlaHsd) and C57BL/6 (C57BL/6JOlaHsd) mice were purchased from Envigo. Ubi- GFP C57BL/6- Tg(UBC- GFP)30Scha/J mice (004353) and B6;129-Cd3e^{tm1Lov}/J mice (004177) were obtained from the Jackson Laboratory. K5-TOM mice were obtained by crossing of KRT5-Cre^{ERT2} knock-in mice [1] with Rosa26-tdTomato mice on mixed background (originally Gt(ROSA)26Sor^{tm1(CAG-tdTomato)Hze}/J mice – 007909, Jackson Laboratory). B6.Cg-Commd10^{Tg(Vav1-cre)A2Kio}/J (008610, Jackson laboratory) were crossed to Rosa26-tdTomato mice to obtain VAV1-TOM mice. LysM-TOM mice were created by crossing of B6.129P2-Lyz2^{tm1(cre)If0}/J (004781, Jackson Laboratory) with Rosa26-tdTomato mice. B6.129P2(C)-Cx3cr1^{tm2.1(cre/ERT2)Jung}/J (020940, Jackson Laboratory) were bred with Rosa26-tdTomato mice and B6.129P2-Gt(ROSA)26Sor^{tm1(DTA)Lky}/J (009669, Jackson Laboratory) to generate Cx3cR1-TOM and Cx3cR1-DTA mice, respectively. Tamoxifen citrate containing mouse chow at a treatment dosage of 400mg/kg (TD.55125, Envigo) was used to activate the CreERT2 protein, thereby inducing Cre recombinase activity in K5-TOM, Cx3cR1^{creER}-TOM and Cx3cR1^{creER}-DTA. The duration of treatment is indicated within each experiment. Mice were either sacrificed by CO₂ asphyxiation or by total exsanguination and excision of the heart under deep isoflurane sedation combined to intraperitoneal anaesthesia (xylazine 10% and ketamine 5% in phosphate-buffered saline (PBS)).

Heterotopic Tracheal Transplantation model. HTT was performed by adapting the murine model developed by Hertz et al. (19) and has already been used in our laboratory as described by Lemaitre et al [2]. Briefly, donor hearts and lungs were exposed through extended median

sternotomy, thymus and heart were dissected away. The trachea was separated from the oesophagus by blunt dissection, excised from the first tracheal ring to the main bronchi and placed in 0.9% sodium chloride until transplantation. Recipient mice were anaesthetized with a mixture of xylazine 10% and ketamine 5% in PBS. A 3 mm incision was made through the dermis posteriorly, at the cervico-thoracic junction, and two small subcutaneous pouch (1.5 x 0.5 cm) were created by blunt dissection on the right and left side of the incision. Each recipient received two tracheas (one for each pouch) in order to reduce the total number of mice needed for the experiments.

Tacrolimus treatment and blood concentration. HTT recipient mice received an intraperitoneal injection of 1 mg/kg/day of tacrolimus (FK506, ab120223, Abcam) from the day of transplantation until harvesting. The control group received vehicle only (DMSO 1.125%, Tween80 4%, PEG400 5.5% in PBS). All injections were performed under gaseous anaesthesia (isoflurane 3%) in order to avoid any damage to the dorsal grafts during mice manipulation and reduce the stress induced by daily injections. Blood was taken by terminal cardiac puncture under deep anaesthesia at three hours post tacrolimus or vehicle injection (C3). Whole blood FK506 concentrations were determined by liquid chromatography-mass spectrometry (LC-MS) at Erasme Hospital (ULB, Brussels) according to validated clinical methods.

Histological assessment. All samples were fixed in 4% formaldehyde at 4°C. Paraffin embedding of samples and staining of 4 µm sections with Haematoxylin- Eosin (HE) and Masson's trichrome (MT) were performed by DIAPath-CMMI (Gosselies). Images of murine samples at 100x total magnification were acquired using an HD camera on an Olympus BX43 microscope. Scans of human lungs were obtained with the NanoZoomer 2.0-HT (Hamamatsu) and analysed with NDP.view v2.7.47 software. The histopathological score for epithelial loss and lumen occlusion in murine allografts was established using ImageJ software. Total

luminal area was calculated from the inner edge of tracheal cartilages. The proportion of epithelial loss was estimated based on the perimeter of the lamina reticularis.

Human samples. Paraffin-embedded samples were obtained from lung explants of patients undergoing a second transplant for BOS. Only samples with histological confirmation of OB lesions were further analysed by immunofluorescence ($n = 10$ patients). Specimens showing healthy peripheral tissue from patients undergoing pulmonary resection for well delimited carcinoid tumor were used as controls ($n = 7$ patients). More information about clinical samples are shown in Supplementary information (Table S1).

Immunofluorescence and confocal analysis. *IF-Frozen.* All murine samples were fixed in 4% PFA for 2 hours, then washed in PBS three times for 15min, and cryoprotected in 30% sucrose/PBS overnight before embedding in OCT (Tissue-Tek). Afterwards, 10 μ m cryosections were washed in PBS (2x 7min), permeabilized with 0.25% Triton X-100/PBS (2x 5min), then blocked for 3 hours at room temperature in an optimized blocking solution (PBS with 6.5% goat serum, 6.5% donkey serum, 5% bovine serum albumin, 5% horse serum, 0.1% Tween20), which was also used to dilute antibodies. Primary antibodies were incubated overnight at 4°C in humid chambers at the following dilutions: rabbit anti-human/mouse α SMA (1:100, polyclonal, Abcam, Ab5694), AF700 rat anti-mouse CD11b (1:50, M1/70, , BD, 557660), rat anti-mouse CD45 (1:100, I3/2.3, Abcam, ab25386), APC rat anti-mouse EpCAM/CD326 (1:50, G8.8, BD, 563478), BV750 rat anti-mouse F4/80 (1:50, T45-2342, BD, 747295), rabbit anti-mouse proCollagen1a1 (1:100, polyclonal, Invitrogen, PA5-35379). Sections were washed three times for 5min each in PBS, incubated with secondary antibodies solution for 2 hours at room temperature in the dark. The following conjugated antibodies were used: AF488 donkey anti-rabbit IgG (1:1000, A21206), AF594 donkey anti-rat IgG (1:500, A21209), AF594 donkey anti-rabbit IgG (1:1000, A21207), AF647 donkey anti-rabbit IgG (1:1000, A21247), AF647 goat anti-rat IgG (1:500, A31573),

all purchased from ThermoFisher Scientific. All antibodies had been centrifuged at 1300 RCF for 2.5 minutes before using to get rid of eventual aggregates. The slides were then washed 10min in PBS, incubated with 0.1% DAPI/PBS for 5min, rinsed with 20mM Tween20 in Tris Buffered Saline (TBS-T) for 10 minutes and mounted with 2.5% Dabco antifade reagent (D2522, Sigma-Aldrich) in Glycergel mounting medium (C0563, Agilent). All samples were protected from direct light exposure during the whole procedure to prevent the fading of spontaneous GFP and tdTomato signal. No anti-GFP or anti-tdTomato antibodies were used in order to avoid false positives from non-specific immunoglobulin binding.

IF-Paraffin. 4μm-thick paraffin-embedded sections from human lungs were deparaffinized with baths of xylene and ethanol, then washed in distilled water. Antigen retrieval was performed in 10mM Citric Acid Buffer (pH 6.0) heated in a microwave at 750W for 15 minutes. After washing in distilled water, all sections were permeabilized with 0.25% Triton X100/PBS (2x 5min), then incubated with optimized blocking solution (PBS with 10% donkey serum, 5% bovine serum albumin, 5% horse serum, 0.1% Tween20) for 2 hours. The same blocking solution was used to dilute antibodies, which had been centrifuged (1300 RCF for 2.5min) before use. Primary antibodies were applied over night at 4°C at the following dilutions: rabbit anti-human/mouse αSMA (1:50, polyclonal, Abcam, Ab5694), mouse anti-human CD45 (1:50, MEM-28, Abcam, ab8216), mouse anti-human CD68 (1:50, KP1, Abcam, ab955). Sections were washed three times in PBS, then stained with the following secondary antibodies for 2 hours at room temperature in the dark: AF488 donkey anti-rabbit IgG (1:500, A21206) and AF594 donkey anti mouse (1:500, A21203), both from ThermoFisher Scientific. After washing in PBS (5min) and TBS-T (5min) the slides were incubated with 0.1% Sudan Black in 70% isopropanol in the dark, then rinsed with distilled water two times for 5min. Nuclei were stained with 0.1% DAPI/PBS. After washing in TBS-T for 10min, all sections were mounted with 2.5% Dabco/Glycergel.

Immunohistochemistry. Immunohistochemical stainings of allografts from Cx3cR1^{CREER}-DTA recipients and controls with Anti-CD3ε monoclonal antibody (clone 2GV6, Roche 05 278 422 001) were performed by DIAPath-CMMI (Gosselies). Four-µm-thick sections were subjected to standard IHC on Ventana discovery XT (Ventana, Roche Diagnostics, Belgium) using the DISCOVERY ChromoMap DAB Kit according to manufacturer's recommendations. Briefly, the formalin-fixed-paraffin-embedded tissues sections, mounted on Superfrost slides, were deparaffinised and rehydrated. Antigen retrieval was performed for 36min using Cell Conditioning 1 (Roche Diagnostics). The slides were incubated with the rabbit monoclonal anti-CD3 antibody for 12min (RTU antibody, clone 2GV6 from Ventana, Roche Diagnostics, Belgium), then washed and incubated for 12min with the anti-rabbit IgG DAB detection system (RTU, DISCOVERY OmniMap anti-Rb, Ventana, Roche Diagnostics, Belgium). Immunostainings were detected by incubation with diaminobenzidine and hydrogen peroxide. All immunohistochemistry slides were counterstained with Gill's hematoxylin, dehydrated and mounted. For each staining, an external positive control was included as well as a negative control (omitting the primary antibody).

Confocal analysis. All images were acquired with a Zeiss LSM 710 confocal microscope in Best Signal mode in order to reduce the risk of signal overspilling and false colocalisation. Pictures were analysed and manually quantified using Zen 2.3 lite Blue software in grid mode (150% digital zoom). For colocalisation of multiple signals, the number of positive cells for each channel was assessed sequentially in each square of the grid by displaying DAPI staining with one channel at the time in order to better identify live cells expressing multiple markers. For each channel, the same values of black and white were employed to all samples in the same experiment. GFP-negative and tdTomato-negative sections were used as negative controls in Ubi-GFP, K5-TOM, VAV1-TOM, LysM-TOM and Cx3cR1-TOM experiments. Furthermore, for all experiments samples incubated only with secondary antibodies or with

DAPI were used as negative controls as well. This allowed to exclude non-specific staining due to secondary antibodies or fluorescent tissue background. For murine samples, tile scan acquisition with autofocus mode (200x total magnification with 0.6 digital zoom per tile) was performed in order to acquire the whole airway in one picture, except for allografts shown in Figure 1 and 2, for which four separate fields (200x, 0.6 digital zoom) overall including the whole section were acquired. Quantification of co-localizing signals was assessed exclusively in the luminal area, delimited by the inner edges of tracheal cartilages. Human lungs quantification was carried out on four random fields (200x, 0.6 digital zoom) per sample. Were excluded from cell count: 1) α SMA⁺ smooth muscle cells; 2) cells with apoptotic or no visible nucleus (showed by DAPI staining); 3) non-specific cell-surface signals detected in channels used for cytoplasmic markers; 4) cytoplasmic signals from surface-only markers, often caused by necrotic debris and red blood cells.

Immunohistochemical quantification. Digitization of tissue sections stained with anti-CD3 ε antibodies were performed using the Hamamatsu Nanozoomer® (zoom 20x). Image processing and analysis were performed using Visiomorph DP 2020.1 (Visiopharm, Hoersholm, Denmark) to determine the positively and negatively stained cells and calculate the fraction of positively stained cells over the whole surface of the lumen.

Flow cytometry. Tracheal grafts were minced and incubated at 37°C (5% CO₂) for 2 hours with 2mg/ml Collagenase A (Merck) in 5% FCS/RPMI and filtered on a 100 μ m strainer. The two allografts harvested from the same recipient were pooled together to increase the total number of cells analysed for each sample. Single bone marrow cells were dissociated with a syringe. Spleens were mechanically separated into single-cell suspensions. All samples were incubated with ACK for RBC lysis, stained to exclude dead cells (Live/Dead Fixable Aqua Dead Cell Stain Kit, for 405 nm excitation, Life Technologies or ViaKrome 808 fixable viability Dye, for infrared 808 nm excitation, Beckman Coulter), incubated with rat anti-

mouse CD16/CD32 (BD 553141, clone 2.4G2, 1:100) and labelled for surface markers for 30min at 4°C in the dark. After fixation and permeabilization with CytoFix/CytoPerm (BD Biosciences) cells were stained for intracytoplasmic markers for 20 minutes in the dark. All cytometric analysis were performed on a Cytoflex-LX cytometer and analysed with FlowJo10 software, except for VAV1-TOM bone marrows for which a Cyan-LX cytometer was used. Combined anti-mouse CD19, CD3ε and NK1.1 staining was used for lineage (LIN) negative selection of B cells, T cells and NK cells in some experiments. Anti-mouse CD11b (AF700, M1/70, 1:100, 557660), CD11c (APC, HL3, 1:100, 550261), CD19 (APC-Cy7, 1D3, 1:100, 557655; PE-Cy7, 1D3, 1:100, 552854), CD3ε (APC-Cy7, 145-2C11, 1:100, 55759), CD45 (BV421, 30-F11, 1:200, 563890; BV650 30-F11, 1:200, 563410; BV510, 30-F11, 1:200, 563891), CD64 (AF647, X54-5/7.1, 1:100, 558939), Ly6C (FITC, AL-21, 1:100, 553104; BV421, AL-21, 1:100, 562727), Ly6G (PerCp-Cy5.5, 1A8, 1:100, 560602; BV650, 1A8, 1:100, 740554), F4/80 (BV750, T45-2342, 1:50, 747295), NK1.1 (APC-Cy7, PK136, 1:100, 560618; PerCP-Cy5.5, 1:100, 551114) were purchased from BD Bioscience. Anti-mouse EpCAM/CD326 (APC-Cy7, G8-8, 1:100, 118218), CD68 (BV711, FA-11, 1:50, 137029) and Cx3cR1 (PE-Cy7, SA011F11, 1:100, 149016) were obtained from Biolegend. Anti-mouse αSMA (FITC, 1A4, 1:50, F3777) was purchased from Sigma-Aldrich.

FACS sorting and scRNA-seq analysis. Single-cell suspension from ten BALB/c-to-LysM-TOM allografts and one LysM-TOM spleen were obtained as per flow cytometry protocol. According to 10X Genomics sample preparation protocol all samples were additionally filtered on a 40μm strainer to avoid 10X microfluidic channel clotting. Cells were stained to exclude dead cells (Live/Dead, Life Technologies) and tdTomato⁺ cells were sorted on a BD FACSaria III using tdTomato⁻ allografts as controls. Microscope assessment after Trypan blue staining allowed to count viable cells following FACS sorting. Cell preparations were centrifuged at 500 RCF for 7 min and pellets were resuspended in 10%FCS/RPMI medium.

Cells were loaded on the Chromium Controller (10x Genomics) and Single-cell RNA-seq libraries were prepared using the Chromium Single Cell 3' v2 Reagent Kit (10x Genomics) according to manufacturer's protocol. Libraries were loaded to an Illumina Novaseq (Brightcore platform, <http://www.brightcore.be/>), and Cell Ranger (10x Genomics) functions mkfastq and count were used to demultiplex the sequencing data and generate gene-barcode matrices. We regressed out mitochondrial and ribosomal genes using SCTtransform function with default parameters from Seurat R package (version 3.1.2)[3]. Contaminant cells (T and B cells) were removed from the analyses. Principal component analysis was performed with default parameters and used in UMAP analysis to identify clusters. We applied FindAllMarkers function to identify differentially expressed genes in each cluster as compared to all other clusters (Wilcoxon Rank Sum test). The differentially expressed genes were used to annotate cells populations which were subject to differential expression analysis between the two organs. AUCell R package [4] was used to identify cells with an active gene set (i.e. gene signatures) in our single-cell RNA-seq data. AUCell uses the “Area Under the Curve” (AUC) to determine if a critical subset of the input gene signature is upregulated within the expressed genes for each cell.

Statistical analysis. GraphPad Prism software v6.01 was used for statistical analysis. Comparisons between two data sets were performed using Mann-Whitney non parametric t-test. Kruskal-Wallis test with Dunn's multiple comparisons test were used when comparing more than two groups. Correlation analyses were done by using Spearman's correlation test.

Study approval. All animal work was carried out in compliance with and after approval by the institutional Animal Care and local committee for Animal Welfare from the Biopark ULB Charleroi (BUC) (P2016/93, #LA1500474). All human *ex vivo* analysis were approved by the ethics committee of Erasme Hospital, ULB, Brussels (P2019/377) and were in accordance with the guidelines outlined by the board. Human samples were obtained from Erasme

Hospital biobank (BE_BERA1; Biobanque Hôpital Erasme-ULB (BERA); BE_NBWB1; Biothèque Wallonie Bruxelles (BWB); BBMRI-ERIC).

References

1. Van Keymeulen A, Rocha AS, Ousset M, Beck B, Bouvencourt G, Rock J, Sharma N, Dekoninck S, Blanpain C. Distinct stem cells contribute to mammary gland development and maintenance. *Nature* 2011; 479: 189–193.
2. Lemaître PH, Vokaer B, Charbonnier L, Iwakura Y, Estenne M, Goldman M, Leo O, Remmelink M, Le Moine A. Cyclosporine A Drives a Th17- and Th2-Mediated Posttransplant Obliterative Airway Disease. *Am. J. Transplant.* 2013; 1: 611–620.
3. Satija R, Farrell JA, Gennert D, Schier AF, Regev A. Spatial reconstruction of single-cell gene expression data. *Nat. Biotechnol.* 2015; 33: 495–502.
4. Aibar S, González-Blas CB, Moerman T, Huynh-Thu VA, Imrichova H, Hulselmans G, Rambow F, Marine JC, Geurts P, Aerts J, Van Den Oord J, Atak ZK, Wouters J, Aerts S. SCENIC: Single-cell regulatory network inference and clustering. *Nat. Methods* 2017; 14: 1083–1086.

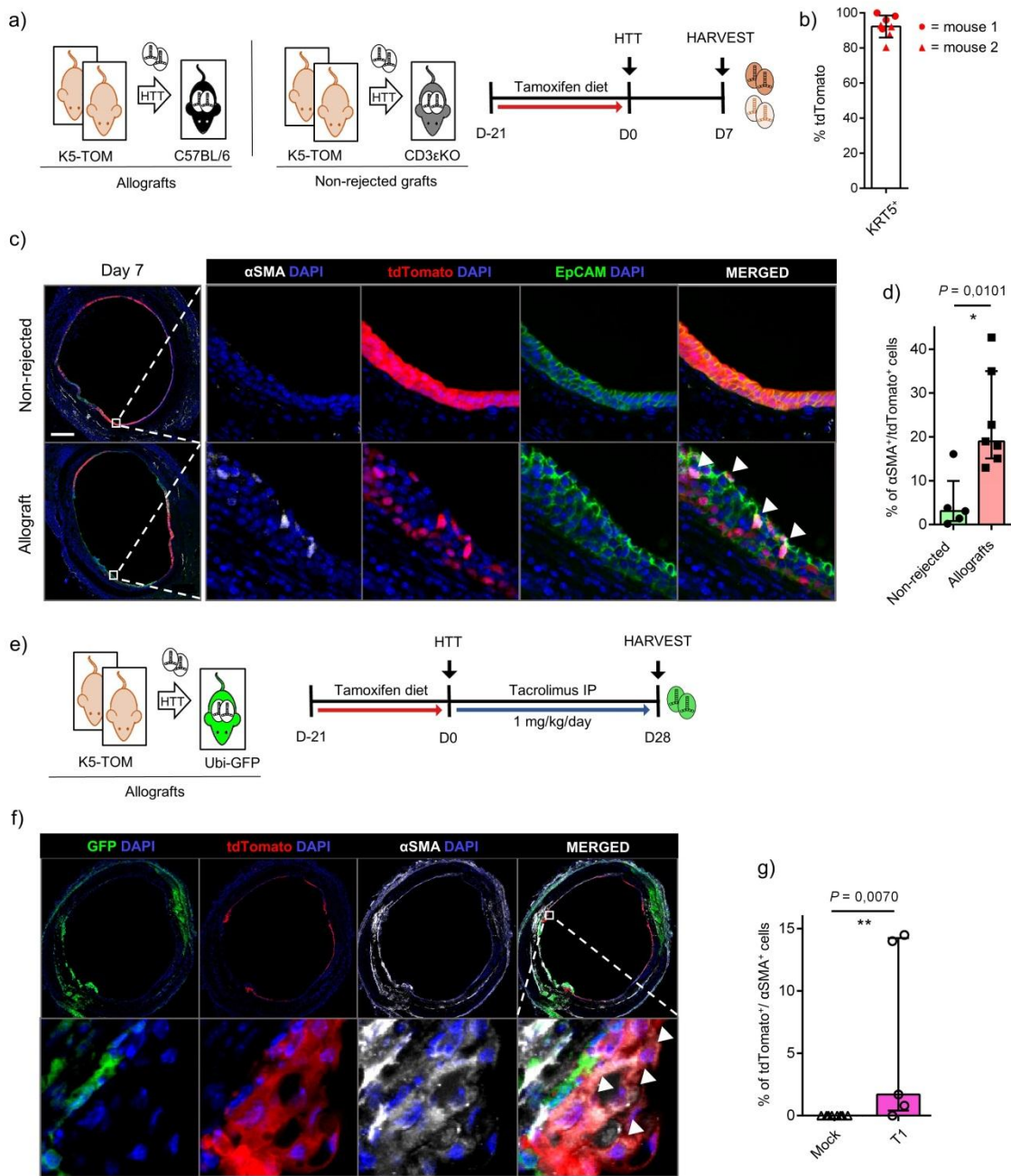


Figure S1. EMT phenomena are found in the allografts at early stages of OAD and at later stages under tacrolimus treatment

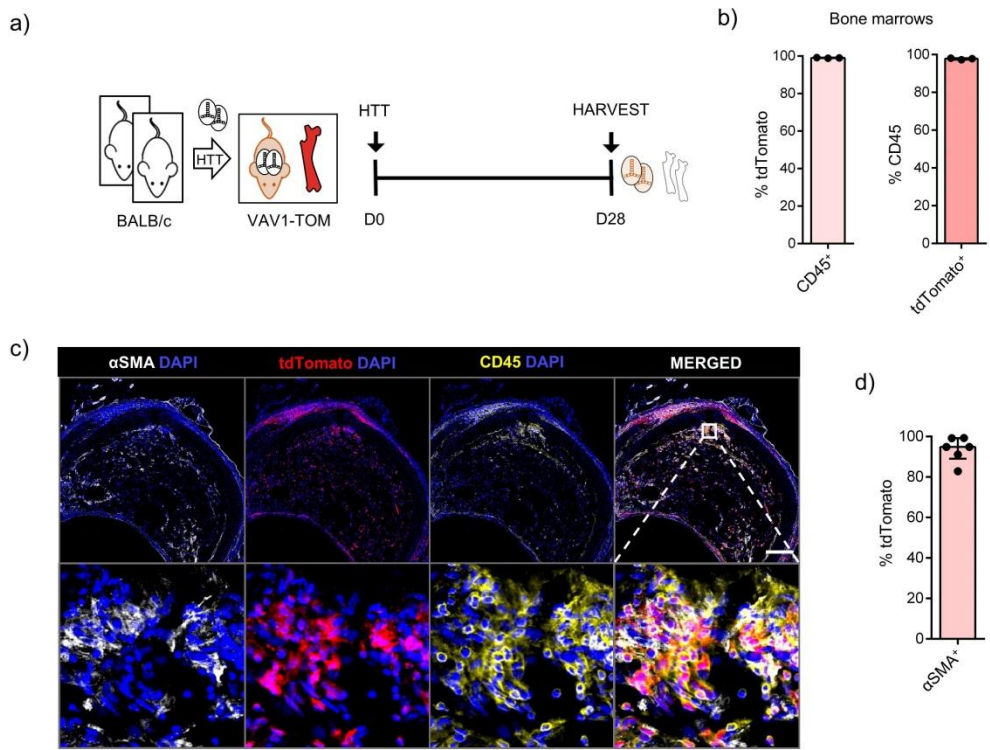


Figure S2. Most myofibroblasts arise from recipient-derived hematopoietic cells.

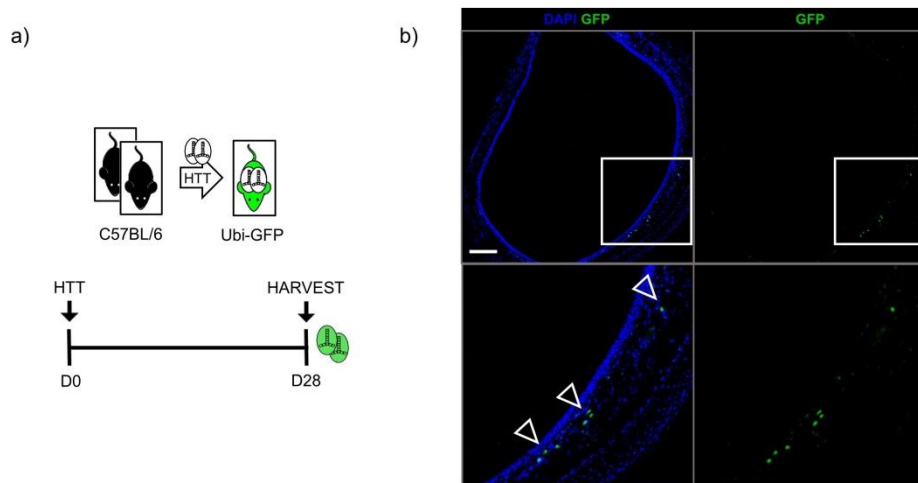
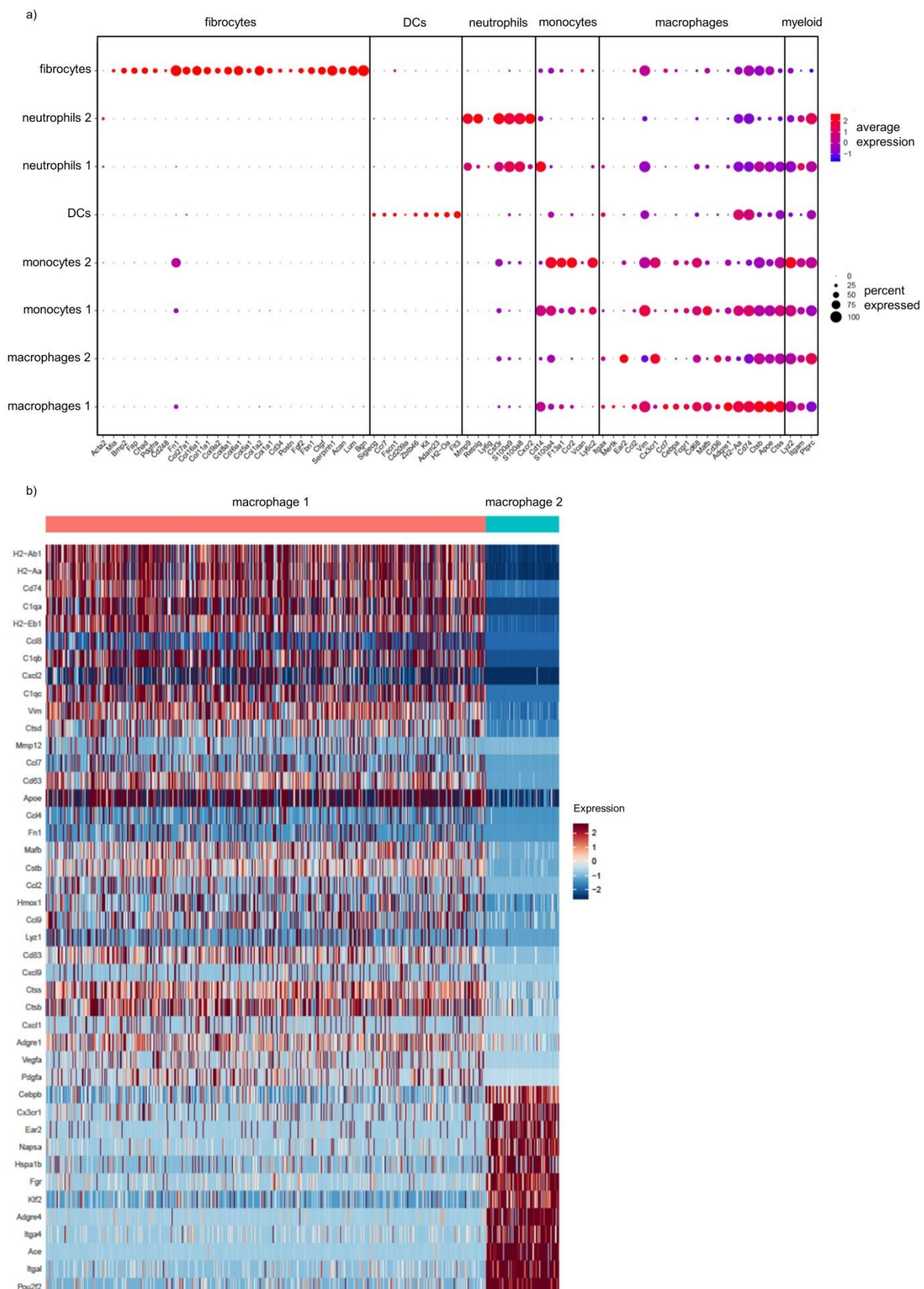
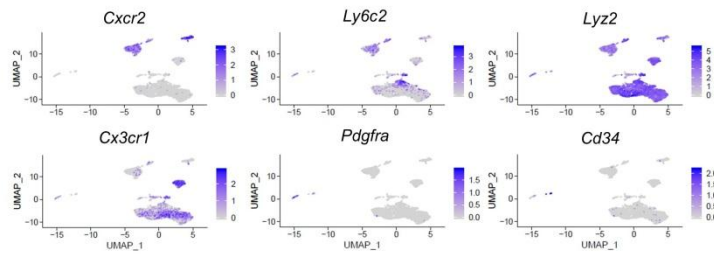


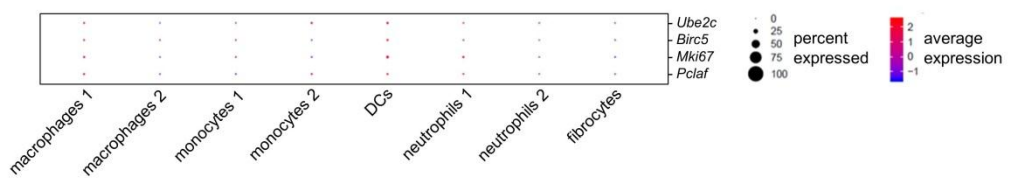
Figure S3. Confocal analysis of syngeneic grafts from UbiGFP recipients at day 28 post-HTT.



c)



d)



Supplementary Figure S3. ScRNA-seq analysis of tdTomato⁺ cells from LysM-TOM spleen and allografts.

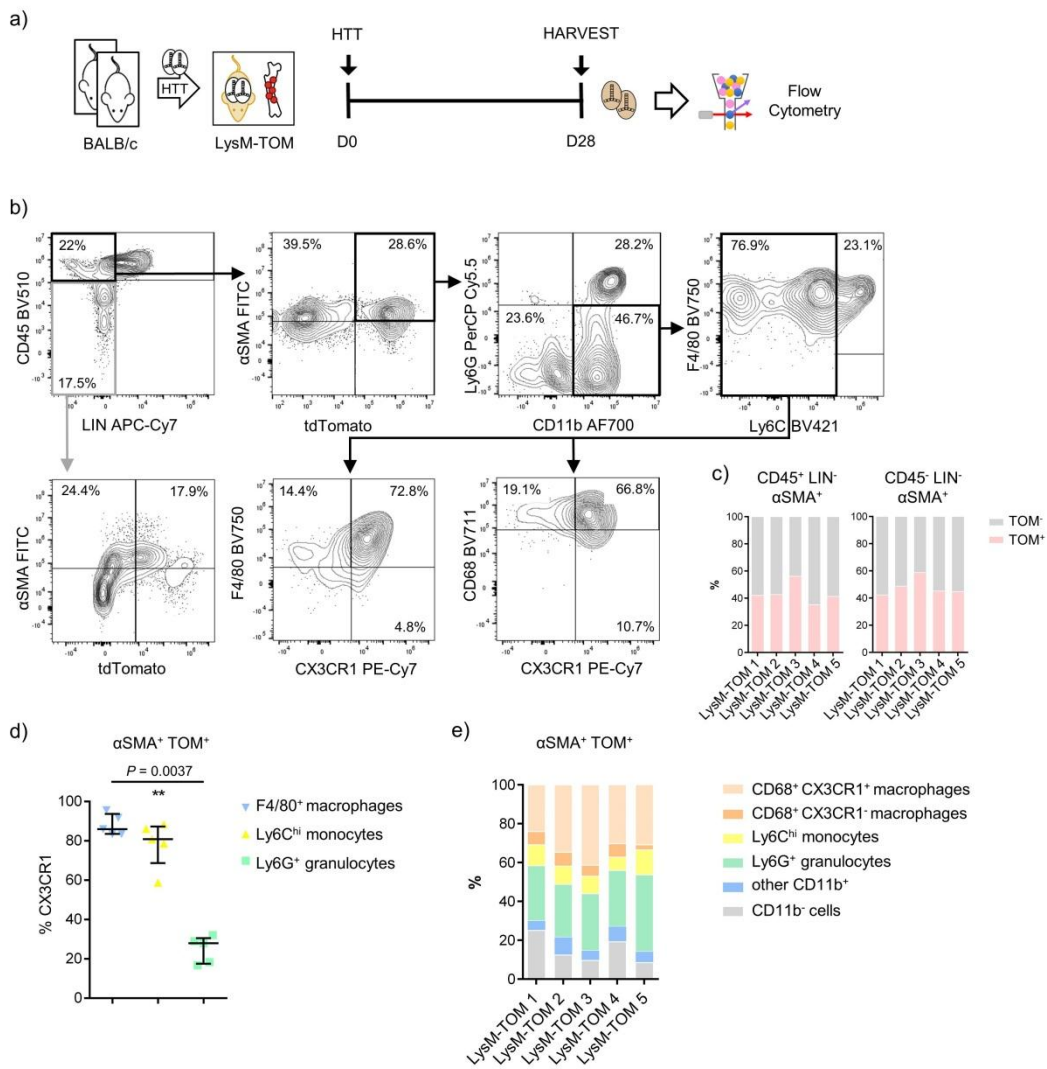


Figure S5. Phenotypic characterization of myeloid-derived α SMA⁺ cells by flow cytometry.

Table S1. Characteristics of lung samples from BOS patients and controls.

ID Sample	age	sex	Cause of lung resection	Histopathologic findings
BOS1	56	M	ReTx for BOS	OB
BOS2	40	M	ReTx for BOS	OB
BOS3	52	F	ReTx for BOS	OB
BOS4	24	M	ReTx for BOS	OB
BOS5	48	M	ReTx for BOS	OB
BOS6	43	F	ReTx for BOS	OB
BOS7	36	F	ReTx for BOS	OB
BOS8	49	F	ReTx for BOS	OB
BOS9	22	F	ReTx for BOS	OB
BOS10	21	M	ReTx for BOS	OB
Control1	60	F	Carcinoid tumor	Normal lung*
Control2	50	F	Carcinoid tumor	Normal lung*
Control3	62	F	Carcinoid tumor	Normal lung*
Control4	65	F	Carcinoid tumor	Normal lung*
Control5	59	F	Carcinoid tumor	Normal lung*
Control6	57	F	Carcinoid tumor	Normal lung*
Control7	38	F	Carcinoid tumor	Normal lung*

ReTx: re-transplantation; BOS: bronchiolitis obliterans syndrome; OB: obliterans bronchiolitis.

*Peripheral lung tissue, distant from the carcinoid lesion